AD-A124 364 ELECTRICALLY SMALL ANTENNAS(U) OHIO STATE UNIV COLUMBUS 1/1
ELECTROSCIENCE LAB J H RICHMOND ET AL. DEC 82
ESL-711964-7 ARO-16258.7-EL DAAG29-79-C-0082

UNCLASSIFIED F/G 9/5 NL

END
DATE
FILMED
DTIC

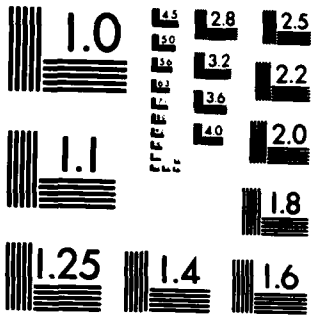

MICROCOPY RESOLUTION TEST CHART
NATIONAL BUREAU OF STANDARDS-1963-A

(12)

OSU

The Ohio State University

ADA124364

ELECTRICALLY SMALL ANTENNAS

J.H. Richmond and C.H. Walter

The Ohio State University

ElectroScience Laboratory

Department of Electrical Engineering
Columbus, Ohio 43212

Final Report 711964-7

Contract No. DAAG29-79-C-0082

December 1982

Department of the Army
U.S. Army Research Office
Research Triangle Park, North Carolina 27709

NOTICES

When Government drawings, specifications, or other data are used for any purpose other than in connection with a definitely related Government procurement operation, the United States Government thereby incurs no responsibility nor any obligation whatsoever, and the fact that the Government may have formulated, furnished, or in any way supplied the said drawings, specifications, or other data, is not to be regarded by implication or otherwise as in any manner licensing the holder or any other person or corporation, or conveying any rights or permission to manufacture, use, or sell any patented invention that may in any way be related thereto.

Unclassified

SECURITY CLASSIFICATION OF THIS PAGE (When Data Entered)

(12)

AD-A124 364

REPORT DOCUMENTATION PAGE

READ INSTRUCTIONS BEFORE COMPLETING FORM

1. REPORT NUMBER: 16258.7-EL	2. GOVT ACCESSION NO.: AD-A124 364
3. RECIPIENT'S CATALOG NUMBER	
4. TITLE (and Subtitle): Electrically Small Antennas	5. TYPE OF REPORT & PERIOD COVERED: Final: 1 May 79 - 30 Oct 82
	6. PERFORMING ORG. REPORT NUMBER
7. AUTHOR(s): J. H. Richmond, C. H. Walter	8. CONTRACT OR GRANT NUMBER(s): DAAG29 79 C 0082
9. PERFORMING ORGANIZATION NAME AND ADDRESS: Ohio State University, Columbus, OH 43212	10. PROGRAM ELEMENT, PROJECT, TASK AREA & WORK UNIT NUMBERS
11. CONTROLLING OFFICE NAME AND ADDRESS: U. S. Army Research Office, Post Office Box 12211, Research Triangle Park, NC 27709	12. REPORT DATE: Dec 82
	13. NUMBER OF PAGES: 45
14. MONITORING AGENCY NAME & ADDRESS (if different from Controlling Office)	15. SECURITY CLASS. (of this report): Unclassified
	15a. DECLASSIFICATION/DOWNGRADING SCHEDULE

16. DISTRIBUTION STATEMENT (of this Report)

Approved for public release; distribution unlimited.

DTIC FEB 15 1983 H

17. DISTRIBUTION STATEMENT (of the abstract entered in Block 20, if different from Report)

18. SUPPLEMENTARY NOTES

The view, opinions, and/or findings contained in this report are those of the author(s) and should not be construed as an official Department of the Army position, policy, or decision, unless so designated by other documentation

19. KEY WORDS (Continue on reverse side if necessary and identify by block number)

small antennas	flat earth
moment methods	microstrip antennas
proximity effects	K-pulse
wire antennas	edge mode

20. ABSTRACT (Continue on reverse side if necessary and identify by block number)

This final report summarizes the work on ARO Grant Number DAAG29 79 C 0082 from 1 May 1979 to 30 October 1982. The purpose of this grant is to develop theory and techniques for small antennas mounted on structures, for microstrip antennas, and for k-pulse applications.

DTIC FILE COPY

DD FORM 1 JAN 73 1473 EDITION OF 1 NOV 65 IS OBSOLETE

UNCLASSIFIED

SECURITY CLASSIFICATION OF THIS PAGE (When Data Entered)

50272-101

REPORT DOCUMENTATION PAGE

1. REPORT NO.

2.

3. Recipient's Accession No.

4. Title and Subtitle

ELECTRICALLY SMALL ANTENNAS

5. Report Date

December 1982

6.

7. Author(s)

J.H. Richmond and C.H. Walter

8. Performing Organization Rept. No.

ESL 711964-7

9. Performing Organization Name and Address

The Ohio State University ElectroScience Laboratory
Department of Electrical Engineering
Columbus, Ohio 43212

10. Project/Task/Work Unit No.

11. Contract(C) or Grant(G) No

(C)

(G) DAAG29-79-C-0082

12. Sponsoring Organization Name and Address

Department of the Army
U.S. Army Research Office
Research Triangle Park, North Carolina 27709

13. Type of Report & Period Covered

Final
5/1/79-10/30/82

14.

15. Supplementary Notes

16. Abstract (Limit: 200 words)

This final report summarizes the work on ARO Grant Number DAAG29-79-C-0082 from 1 May 1979 to 30 October 1982. The purpose of this grant is to develop theory and techniques for small antennas mounted on structures, for microstrip antennas, and for k-pulse applications.

DTIC COPY INSPECTED 8

Accession For
NTIS GRA&I
DTIC TAB
Unannounced
Justification
By
Distribution/
Availability Codes
Avail and/or
Dist Special
A

17. Document Analysis a. Descriptors

Small antennas
Moment methods
Proximity effects
Wire Antennas
Flat Earth
Microstrip antennas
K-Pulse
Edge mode

b. Identifiers/Open-Ended Terms

c. COSATI Field/Group

18. Availability Statement

DISTRIBUTION STATEMENT A
Approved for public release;
Distribution Unlimited

19. Security Class (This Report)

Unclassified

20. Security Class (This Page)

Unclassified

21. No. of Pages

45

22. Price

(See ANSI-Z39.18) See Instructions on Reverse OPTIONAL FORM 272 (4-77) (Formerly NTIS-35) Department of Commerce

TABLE OF CONTENTS

	Page
BRIEF OUTLINE OF RESEARCH FINDINGS	3
APPENDIX	
A. MUTUAL IMPEDANCE BETWEEN VERTICAL DIPOLES OVER A FLAT EARTH	7
B. ON THE EDGE MODE IN THE THEORY OF TM SCATTERING BY A STRIP OR STRIP GRATING	11
C. ON THE EDGE MODE IN THE THEORY OF THICK CYLINDRICAL MONOPOLE ANTENNAS	17
D. FIELD OF SEPARABLE ELECTRIC SOURCE CURRENT DISTRIBUTION IN FREE SPACE	24
E. SCATTERING FROM CYLINDRICAL INHOMOGENEITIES IN A LOSSY MEDIUM	28
F. PROPAGATION OF SURFACE WAVES ON A BURIED COAXIAL CABLE WITH PERIODIC SLOTS (ABSTRACT)	44

FINAL REPORT

1. ARO PROPOSAL NUMBER: 08542-55-00

2. PERIOD COVERED BY REPORT: May 1, 1979 - October 30, 1982

3. TITLE OF PROPOSAL: "Electrically Small Antennas"

4. CONTRACT OR GRANT NUMBER: DAAG29-79-C-0082

5. NAME OF INSTITUTION: The Ohio State University
Department of Electrical Engineering
ElectroScience Laboratory
Columbus, Ohio 43212

6. AUTHOR(S) OF REPORT: J.H. Richmond and C.H. Walter

7. LIST OF MANUSCRIPTS SUBMITTED OR PUBLISHED UNDER ARO SPONSORSHIP DURING THIS PERIOD, INCLUDING JOURNAL REFERENCES:

(NOTE: Copies of the journal publications are included in the appendices.)

J.H. Richmond and E.H. Newman, "Mutual Impedance Between Vertical Dipoles Over a Flat Earth", Radio Science, Vol. 14, pp. 957-959, November-December 1979.

J.H. Richmond, "On the Edge Mode in the Theory of TM Scattering by a Strip or Strip Grating", IEEE Trans., Vol. AP-28, pp. 883-887, November 1980.

J.H. Richmond, "On the Edge Mode in the Theory of Thick Cylindrical Monopole Antennas", IEEE Trans., Vol. AP-28, pp. 916-921, November 1980.

J.H. Richmond, "Field of Separable Electric Source Current Distribution in Free Space", Radio Science, Vol. 16, pp. 1299-1301, November-December 1981.

L. Peters, Jr. and J.H. Richmond, "Scattering from Cylindrical Inhomogeneities in a Lossy Medium", Radio Science, Vol. 17, pp. 973-987, September-October 1982.

J.H. Richmond, "Propagation of Surface Waves on a Buried Coaxial Cable with Periodic Slots", submitted for publication in IEEE Trans. on Electromagnetic Compatibility.

E.M. Kennaugh and J.H. Richmond, "K-Pulse Waveforms for Cylindrical-Wire Antenna with Lumped Load", Manuscript in preparation.

8. SCIENTIFIC PERSONNEL SUPPORTED BY THIS PROJECT AND DEGREES AWARDED DURING THIS REPORTING PERIOD:

E.M. Kennaugh
J.H. Richmond
C.H. Walter

No degrees awarded during this period.

BRIEF OUTLINE OF RESEARCH FINDINGS

This final report summarizes the work on ARO Grant Number DAAG29-79-C-0082 from 1 May 1979 to 30 October 1982. The purpose of this grant is to develop theory and techniques for small antennas mounted on structures, for microstrip antennas, and for k-pulse applications.

Much of the research effort during this period is described in the published papers which are reproduced in the Appendices.

First let us summarize our accomplishments related to small antennas mounted on structures.

The theory and computer programs were developed for plane-wave scattering by an infinitely long elliptic cylinder with arbitrary surface impedance. The solution has the form of a series of Mathieu functions. The calculated data show excellent agreement with GTD calculations.

We investigated the characteristic modes of Garbacz and Harrington for conducting strips, strip gratings, thick tubular dipoles, and periodic collinear arrays of thick tubular dipoles. For the conducting strip, it was found the characteristic modes coincide with the eigenmodes of the degenerate elliptic cylinder expressed in terms of Mathieu functions. For periodic structures such as the strip grating and the collinear array of dipoles, when the spacing is less than the wavelength, a single characteristic mode is induced by a plane wave with normal incidence.

In most applications it is difficult to obtain more than three or four of the characteristic modes. In the complex frequency domain, new techniques are required for characteristic modes since the impedance matrix is no longer positive definite. For these reasons, we investigated the conjugate modes of Inagaki. Even in the complex frequency domain, it is always easy to obtain a complete set of conjugate modes. We found that the conjugate modes reduce to the natural modes at the poles of the conducting body. For the strip and the tubular dipole, graphs were plotted to illustrate the lowest-order characteristic modes and the conjugate modes.

We applied the double Fourier transform to develop the theory of thin-wire and thin-strip antennas located on or near the air-earth interface. Previous investigators have used the Fourier-Bessel transform for these problems, but the double Fourier transform has significant advantages. For a thin-strip antenna near the air-earth interface, our technique requires double numerical integration whereas the earlier methods require five-fold numerical integration. The Fourier-Bessel method encounters a singularity when the antenna is on the interface, but the double Fourier transform technique is well behaved in this situation.

Next, we applied the double Fourier transform to calculate the current distribution and impedance of a horizontal strip dipole as a function of distance from the air-earth interface. The calculations include the cases where the dipole is on the interface, buried in the earth, and elevated above the interface. Although the impedance varies

rapidly with distance when the dipole is near the interface, it appears that the impedance is continuous across the interface.

We also considered a skewed strip dipole near the air-earth interface. The skewed dipole is neither vertical nor horizontal, but is oriented at an arbitrary angle with respect to the interface. The double Fourier transform proved quite advantageous for this application. With this approach, the number of Sommerfeld-integral evaluations is reduced by a factor of ten in comparison with the conventional Fourier-Bessel transformation.

Next let us summarize our research accomplishments related to microstrip antennas.

We applied the double Fourier transform to develop the theory of microstrip antennas. In calculating the self impedance of a rectangular microstrip antenna, our new computer code reduces the computational expense by a factor of ten.

In many applications, the patch model of a microstrip antenna will involve trapezoidal patches. Therefore, we considered the mutual impedance of two trapezoidal patches and developed the theory far enough to show that the transform approach is quite feasible for this application.

Finally, let us summarize our research related to k-pulse applications. We extended the k-pulse theory to include the effects of the generator impedance at the transmitting antenna and the load impedance at the receiving antenna. For numerical calculations, we considered two center-fed cylindrical-wire antennas with the following

generator and load impedances: 0, 50, 916, and ∞ ohms. We used the frequency-domain moment method to calculate the antenna impedance and effective length at many frequencies. The effective length was calculated for broadside incidence and also for an angle of 45 degrees away from broadside. From these data we employed the Fourier transform to calculate the following k-pulse waveforms: the generator voltage $v_g(t)$, the incident far-zone field waveform $E_i(t)$, and the received voltage waveform $v_r(t)$. A manuscript is being prepared to present these new results.

APPENDIX A

MUTUAL IMPEDANCE BETWEEN VERTICAL DIPOLES OVER A FLAT EARTH

Radio Science, Volume 14, Number 6, pages 957–959, November–December 1979

Mutual impedance between vertical dipoles over a flat earth

J. H. Richmond and E. H. Newman

The Ohio State University ElectroScience Laboratory, Department of Electrical Engineering, Columbus, Ohio 43212

(Received January 23, 1979; revised July 11, 1979.)

The fields of a vertical dipole and the mutual impedance between vertical dipoles over a flat earth are expressed in terms of a Sommerfeld integral.

1. INTRODUCTION

The use of vertical wire antennas, or arrays of vertical wires, over the earth is common. This problem can be analyzed by using the method of moments [*Harrington*, 1968], where the effects of the flat earth are accounted for by modifying each element in the impedance matrix. The computation of the modification to a single element in the matrix involves the numerical evaluation of a Sommerfeld integral [*Sommerfeld*, 1964]. With sinusoidal bases and point matching, it has been shown [*Miller et al.*, 1972] that a single evaluation of the Sommerfeld integral suffices for each impedance element. Miller et al. report a computation time of 20 s on a CDC-6600 computer for impedance of a vertical half-wave dipole over the flat earth. In view of this computational expense, they present data based on a 5-segment antenna model, although these data differ by 8% from those with a 21-segment model. They present the theory based on enforcement of the integral equation on the axis of the wire.

In this paper we present the general formulation and show that a single evaluation of the Sommerfeld integral suffices for almost any choice of basis and testing functions. Instead of matching on the axis, we present the theory appropriate for enforcement of the integral equation on the surface of the wire. More accurate data are presented for the impedance of a center-fed vertical wire versus height above the earth, and it is found that our calculations are significantly faster than those quoted above.

2. FIELD OF VERTICAL DIPOLE

For an electric line source located on the z axis in free space the vector potential has only a z component given by

$$A = \int_{z_1'}^{z_2'} \frac{I(z')e^{-jkR}}{4\pi R}\,dz' \tag{1}$$

where z_1' and z_2' denote the end points of the line source and $I(z')$ represents the current distribution with the time dependence $e^{j\omega t}$ suppressed.

By expanding the spherical wave $\exp(-jkR)/R$ in a spectrum of cylindrical waves, we obtain

$$A = \int_0^\infty \beta J_0(\beta\rho)\frac{F(\gamma)e^{\gamma z}}{4\pi\gamma}\,d\beta \tag{2}$$

$$\gamma^2 = \beta^2 - k^2 \tag{3}$$

$$F(\gamma) = \int_{z_1'}^{z_2'} I(z')e^{-\gamma z'}\,dz' \tag{4}$$

where z is less than z_1'. The electric field intensity is given by

$$E_z = \frac{1}{j\omega\epsilon}\left(k^2 A + \frac{\partial^2 A}{\partial z^2}\right) \tag{5}$$

$$E_z = C\int_0^\infty \beta^3 J_0(\beta\rho)(F/\gamma)e^{\gamma z}\,d\beta \tag{6}$$

where $C = -j\eta/(4\pi k)$ and η is the impedance of free space.

Now let the xy plane be the air-earth interface. With the field in (6) incident on the interface the reflected field is given by

$$E_z' = C\int_0^\infty \beta^3 R J_0(\beta\rho)(F/\gamma)e^{-\gamma z}\,d\beta \tag{7}$$

where the reflection coefficient R is a function of γ and the parameters of the earth; (ρ, ϕ, z) denote cylindrical coordinates with origin on the interface and line source on the z axis.

Now consider a tubular vertical dipole with radius 'a,' current distribution $I(z')$, and surface current

Copyright © 1979 by the American Geophysical Union.

0048-6604/79/1112-0957$01.00

density uniformly distributed around the tube. The reflected field for this source is found from (7) by using the addition theorem for the Bessel function and integrating around the surface of the tube:

$$E_z^r = C \int_0^\infty \beta^3 R J_0(\beta a) J_0(\beta\rho)(F/\gamma) e^{-\gamma z} d\beta \tag{8}$$

where ρ is measured from the axis of the tubular source.

3. MUTUAL IMPEDANCE OF VERTICAL DIPOLES

The mutual impedance between tubular vertical dipoles is given by

$$Z_{12} = -\frac{1}{I_1 I_2} \iint J_2 E_1 \, ds \tag{9}$$

I_1 and I_2 denote the terminal currents, and the integration extends over the cylindrical surface of dipole 2. Dipole 2 has radius a_2, current distribution $I_2(z)$, and uniform surface current density J_2 around the tube. The z component of the field of dipole 1 is given by

$$E_1 = E_1^0 + E_1^r \tag{10}$$

where the first term denotes the free-space field and the second term is the field reflected from the interface. From (9) and (10),

$$Z_{12} = Z_{12}^0 + Z_{12}^r \tag{11}$$

where the first term is the mutual impedance in free space and the second term is the change in mutual impedance arising from interface reflection.

Using (8) for the reflected field, invoking the addition theorem, and integrating around the surface of dipole 2, we find

$$Z_{12}^r = -\frac{C}{I_1 I_2} \int_0^\infty \beta^3 (R/\gamma) \cdot J_0(\beta a_1) J_0(\beta a_2) J_0(\beta d) FG \, d\beta \tag{12}$$

$$G(\gamma) = \int_{z_1}^{z_2} I_2(z) e^{-\gamma z} dz \tag{13}$$

The horizontal distance between the dipole axes is denoted by d, and z_1 and z_2 are the end points of dipole 2.

In moment method applications the current distributions $I_m(z')$ and $I_n(z)$ represent the basis functions, and (12) determines Z_{mn}^r. For any simple basis functions it is apparent from (4) and (13) that the functions F and G can be obtained in simple closed form. Thus we see from (12) that a single evaluation of the Sommerfeld integral is sufficient to calculate each of the mutual impedance terms Z_{mn}^r. In the sinusoidal Galerkin formulation the basis and testing functions are

$$I_m(z') = \frac{\sin k(h_m - |z' - z_m'|)}{\sin kh_m} \tag{14}$$

$$I_n(z) = \frac{\sin k(h_n - |z - z_n|)}{\sin kh_n} \tag{15}$$

where h_m and h_n denote the segment lengths. Function m extends over the two segments which intersect at z_m', and function n extends over the two segments which intersect at z_n.

4. NUMERICAL RESULTS

Figure 1 illustrates the impedance of a half-wave center-fed vertical wire. Here h denotes the distance from the air-earth interface to the center of the wire. These data were calculated with the sinusoidal Galerkin formulation. The wire was divided into 30 segments, so there were 29 equations and 29 unknowns. In Figure 1 the trends are similar to

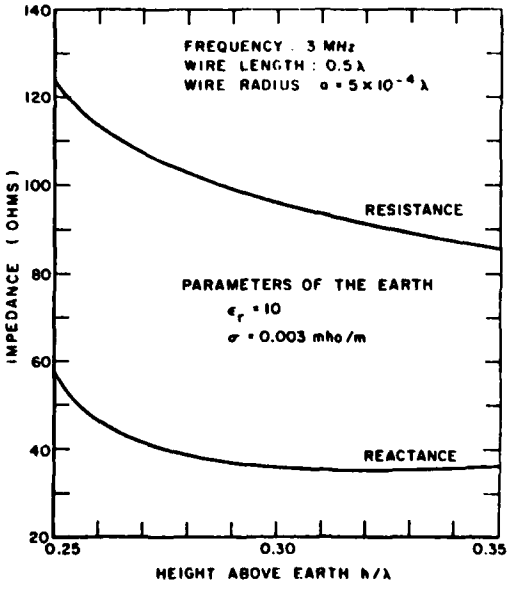

Fig. 1. Impedance of center-fed vertical wire versus height above the earth.

those in Figure 2 of *Miller et al.* [1972], but the data agree more closely with their 21-segment results rather than the 5-segment results they present.

If the 20-s computation time quoted by Miller et al. applies to their 5-segment model, our corresponding 6-segment calculations are 100 times faster. If it applies to their 21-segment model, our 22-segment calculations are 12 times faster. We employed a simple Newton-Cotes integration as opposed to their adaptive integration for the Sommerfeld integral. In addition, our free-space impedance terms Z^0_{mn} are in simple closed form, whereas theirs may require numerical integration.

Surface matching is slower than axis matching, and the two techniques give essentially the same results for wires with small radius as in Figure 1. For larger radii such as the often quoted results for $a = 0.007\ \lambda$, however, surface matching is required for accurate results and, indeed, for convergence.

Acknowledgment. The work reported in this paper was supported in part by contract DAAG29-79-C-0082 between the Department of the Army, U.S. Army Research Office, and The Ohio State University Research Foundation.

REFERENCES

Harrington, R. F. (1968), *Field Computation by Moment Methods*, 229 pp., Macmillan, New York.

Miller, E. K., A. J. Poggio, G. J. Burke, and E. S. Selden (1972), Analysis of wire antennas in the presence of a conducting half-space, 1, The vertical antenna in free space, *Can. J. Phys.*, *50*, 879–888.

Sommerfeld, A. (1964), *Partial Differential Equations in Physics*, 335 pp., Academic, New York.

APPENDIX B

ON THE EDGE MODE IN THE THEORY OF TM SCATTERING BY A STRIP OR STRIP GRATING

On the Edge Mode in the Theory of TM Scattering by a Strip or Strip Grating

JACK H. RICHMOND, FELLOW, IEEE

Abstract—Consider a plane wave incident on a perfectly conducting strip (or strip grating), and let the incident electric vector be parallel with the edges of the strip. If the edge mode is included among the basis functions, it is found this greatly improves the convergence of the moment-method solution. Numerical data are included for the reflection coefficient of the strip grating. To correct an error in the previous literature, the rigorous solution is tabulated for broadside backscatter from a single strip.

I. INTRODUCTION

BIBLIOGRAPHIES on strip gratings are available in [1] and [2], and a chapter on scattering by a strip is included in [3]. For a related geometry, Minor and Bolle [4] include the edge modes in an efficient formulation for shielded microstrip. In scattering by a strip, Shafai and El-Moazzen [5] use a transformation to treat the edge singularities in the current distribution. Tsai *et al.* [6] sample the current function at progressively smaller intervals near the edge. Wilton and Govind [7] incorporate the edge conditions with subsectional bases. In [6] and [7], the objective is to obtain more accurate calculations of the current distribution. Their techniques evidently did not improve the convergence of the solution.

In this paper we develop the theory of scattering for a strip and a strip grating. When the basis functions include the edge mode, it is shown this greatly improves the convergence of the moment-method solution with entire-domain expansion functions. For a strip with width equal to the wavelength, our calculations with three unknowns show excellent agreement with the current distribution obtained in [7] with 25 unknowns. For a strip grating with normal incidence and spacing less than the wavelength, it is found the current distribution has the constant phase property of a characteristic mode [8], [9].

Although our technique shows some similarity to the "asymptotic anticipation method" of Neureuther and Zaki [15], we introduce several improvements. In their discussion of plane wave scattering by a wire mesh, Hill and Wait [16] use related techniques to improve the convergence.

We consider a grating or a strip with perfect conductivity, infinite length, and infinitesimal thickness. The time dependence $e^{j\omega t}$ is assumed and suppressed. At first the current density on the strip is expanded in a Fourier series, and a system of simultaneous linear equations is developed for the Fourier coefficients. Then the current distribution is expressed as the sum of an edge mode plus a Fourier series, and it is found that the simultaneous linear equations can be obtained readily from the previous expressions. The next section considers a strip grating with oblique incidence, but for the sake of brevity the remainder of the paper considers normal incidence.

II. THEORY OF STRIP GRATING WITH OBLIQUE INCIDENCE

Consider a time-harmonic plane wave in free space to have oblique incidence on a periodic planar array of thin conducting strips as in Fig. 1. Each strip has width $w = 2h$ and s denotes the spacing. The z axis coincides with the axis of one of the strips, and the incident electric field intensity is

$$E^i = \hat{z}E_0 e^{jkx\cos\phi}\, e^{jky\sin\phi} \tag{1}$$

Manuscript received November 26, 1979; revised May 27, 1980. This work was supported in part by Contract DAAG29-79-C-0082 between Department of the Army, U.S. Army Research Office, and the Ohio State University Research Foundation.

The author is with the ElectroScience Laboratory, The Ohio State University, Columbus, OH 43212.

0018-926X/80/1100-0883$00.75 © 1980 IEEE

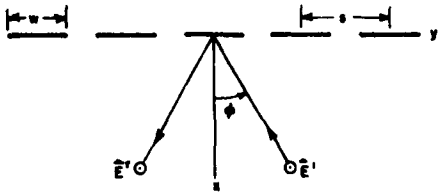

Fig. 1. Plane wave with oblique incidence on strip grating.

where $k = \omega\sqrt{\mu\epsilon}$. The scattered field is

$$\vec{E}^s = \hat{z}E_0 e^{jky\sin\phi} \sum_{-\infty}^{\infty} a_n e^{-\gamma_n|x|} e^{j2n\pi y/s} \tag{2}$$

$$H_y^s = -\frac{E_0 \operatorname{sgn}(x)}{j\omega\mu} e^{jky\sin\phi} \sum_{-\infty}^{\infty} a_n \gamma_n e^{-\gamma_n|x|} e^{j2n\pi y/s} \tag{3}$$

$$\gamma_n^2 = (k\sin\phi + 2n\pi/s)^2 - k^2. \tag{4}$$

where $\operatorname{sgn}(x) = -1$ for $x < 0$, and $+1$ for $x > 0$.

Let us expand the surface-current density on the strips in a Fourier series:

$$\vec{J} = \hat{z}e^{jky\sin\phi} \sum b_l e^{jl\pi y/h}. \tag{5}$$

From the boundary condition on tangential H,

$$E_0 \sum a_n \gamma_n e^{j2n\pi y/s} = \begin{cases} -j0.5k\eta \sum b_l e^{jl\pi y/h}, & -h < y < h \\ 0, & \text{in the apertures} \end{cases} \tag{6}$$

where $\eta = \sqrt{\mu/\epsilon}$. We multiply both sides of (6) by $e^{-j2n\pi y/s}$ and integrate over the region $-s/2 < y < s/2$ to obtain

$$a_0 = -\eta w b_0/(2sE_0 \cos\phi) \tag{7}$$

$$a_n = \frac{-jk\eta}{2s\gamma_n E_0} \sum b_l F_{ln} \tag{8}$$

$$F_{ln} = \int_{-h}^{h} e^{j2\pi(l/w - n/s)y}\, dy. \tag{9}$$

By forcing tangential E to vanish on the conducting strips, we obtain from (1) and (2)

$$\sum a_n e^{j2n\pi y/s} = -1, \qquad -h < y < h. \tag{10}$$

We multiply both sides of (10) by $e^{-jl\pi y/h}$ and integrate over the region $-h < y < h$ to obtain

$$\sum a_n F_{ln}^* = \begin{cases} -w, & \text{if } l = 0 \\ 0, & \text{if } l \neq 0 \end{cases} \tag{11}$$

where an asterisk denotes the complex conjugate and F_{ln} is defined by (9). In (11) let us replace a_n with the equivalent quantity from (7) and (8). This yields the following system of simultaneous linear equations:

$$\sum_l b_l Z_{il} = V_i, \qquad i = 0, \pm 1, \pm 2, \cdots, \tag{12}$$

$$Z_{il} = \frac{jk\eta}{2sw} \sum_n F_{in}^* F_{ln}/\gamma_n \tag{13}$$

where $V_i = 0$ except $V_0 = E_0$.

The reflection and transmission coefficients of the strip grating are given by

$$R = a_0 \tag{14}$$

$$T = 1 + R. \tag{15}$$

To obtain numerical data, we truncate the series in (12) and use matrix inversion to solve these equations for the constants b_l. In view of the basis and testing functions used, (12) and (13) may be considered the "Fourier–Galerkin formulation."

We usually expect the Galerkin formulation to converge faster than a point-matching solution. In this application, however, the two techniques show equal performance. The only advantage of the Galerkin method is that it yields a symmetric matrix Z_{il}. It is, however, a distinct advantage to treat the constants b_l as the unknowns in (12), rather than using the a_n as the unknowns as in [15].

III. STRIP GRATING WITH NORMAL INCIDENCE

For normal incidence ($\phi = 0$), it is convenient to express the scattered field as

$$\vec{E}^s = \hat{z}E_0 \sum_0^{\infty} a_n e^{-\gamma_n|x|} \cos(2n\pi y/s) \tag{16}$$

and the current density as

$$\vec{J} = \hat{z} \sum_0^{N} b_l \cos(l\pi y/h). \tag{17}$$

By enforcing the boundary condition on tangential H (with testing function $\cos 2n\pi y/s$), we find

$$a_n = \frac{-jk\eta w e_n}{s\gamma_n E_0} \sum_0^{N} b_l G_{ln} \tag{18}$$

$$G_{ln} = (1/w) \int_0^h \cos(l\pi y/h) \cos(2n\pi y/s)\, dy \tag{19}$$

where $e_n = 2$ except $e_0 = 1$. By forcing tangential E to vanish on the strips we find

$$\sum_0^{\infty} a_n \cos(2n\pi y/s) = -1, \qquad -h < y < h. \tag{20}$$

Multiplying (20) by $\cos i\pi y/h$ and integrating over the range $0 < y < h$ yields

$$\sum_{n=0}^{\infty} a_n G_{in} = \begin{cases} -0.5, & \text{if } i = 0 \\ 0, & \text{if } i \neq 0. \end{cases} \tag{21}$$

From (18) and (21),

$$\sum_{l=0}^{N} b_l Z_{il} = V_i, \qquad i = 0, 1, 2, \cdots, N \tag{22}$$

$$Z_{il} = (2jk\eta w/s) \sum_{n=0}^{\infty} e_n G_{in} G_{ln} / \gamma_n \tag{23}$$

where $V_i = 0$ except $V_0 = E_0$. The impedance matrix Z_{il} is symmetric. The reflection coefficient is given by $R = a_0$, and a_0 and b_0 are related by (7).

If the incident field is

$$\vec{E}^i = \hat{z} E_0 e^{\gamma m x} \cos(2m\pi y/s),$$

the solution is given by (16)–(19) and (22)–(23) with

$$V_i = 2E_0 G_{im}.$$

IV. STRIP GRATING WITH EDGE MODE

The current distribution $J(y)$ has singularities at the edges of a strip. Thus, when J is expressed as a Fourier series, the series has slow convergence and one must invert a rather large matrix to obtain an accurate solution. To improve the situation, we may express J as the sum of an edge mode (to take care of the singularities) and a Fourier series. In this case the Fourier series should converge rapidly since it represents a well-behaved function.

For normal incidence, a suitable edge mode for the current distribution on a strip is

$$J_e = (I_e/w) \frac{2}{\pi\sqrt{1-(y/h)^2}} \tag{24}$$

$$J_e = (I_e/w) \sum_{0}^{\infty} e_l J_0(l\pi) \cos(l\pi y/h) \tag{25}$$

$$I_e = \int_{-h}^{h} J_e(y)\, dy \tag{26}$$

where $J_0(l\pi)$ denotes the Bessel function. The function J_e has the correct behavior in the neighborhood of each edge of the strip.

For normal incidence, let us express the current density on the strip as the sum of the edge mode and a Fourier series:

$$J_z = J_e + \sum_{0}^{N-1} c_l \cos(l\pi y/h). \tag{27}$$

Using (25) for J_e and comparing (17) and (27), we find

$$b_l = c_l + (I_e/w) e_l J_0(l\pi). \tag{28}$$

From (22) and (28),

$$c_N \sum_{l=0}^{\infty} e_l J_0(l\pi) Z_{il} + \sum_{l=0}^{N-1} c_l Z_{il} = V_i \tag{29}$$

where $c_N = I_e/w$ denotes the amplitude of the edge mode.

Equation (29) can be rearranged as follows:

$$\sum_{l=0}^{N} c_l Z_{il}' = V_i, \qquad i = 0, 1, 2, \cdots, N \tag{30}$$

$$Z_{il}' = Z_{il}, \qquad \text{for } l < N \tag{31}$$

$$Z_{iN}' = \sum_{m=0}^{\infty} e_m J_0(m\pi) Z_{im} \tag{32}$$

where Z_{il} and Z_{im} are given by (23) and $V_i = 0$ except $V_0 = E_0$. The matrix Z_{il}' is not symmetric.

We could obtain a symmetric matrix by using the edge mode (instead of the last cosine term) as a testing function with (20) to derive the last equation ($i = N$) in (30). In this case $Z_{Nm}' = Z_{mN}'$ and $V_i = 0$ except $V_0 = V_N = E_0$. However, slightly better convergence is obtained with the unsymmetric system in (30)–(32).

V. SINGLE STRIP WITH NORMAL INCIDENCE

When a plane wave has normal incidence on a single strip, the scattered field can be expressed as follows:

$$E^s = \hat{z} E_0 \int_0^{\infty} A \cos gy e^{-\gamma|x|}\, dg \tag{33}$$

$$H_y^s = \frac{-E_0 \operatorname{sgn}(x)}{jk\eta} \int_0^{\infty} \gamma A \cos gy e^{-\gamma|x|}\, dg \tag{34}$$

$$\gamma^2 = g^2 - k^2. \tag{35}$$

Let us express the current density on the strip as a Fourier series:

$$\vec{J} = \hat{z} \sum_{0}^{N} b_l \cos(l\pi y/h). \tag{36}$$

(The edge mode will be introduced later.) The boundary condition on tangential H leads to

$$\int_0^{\infty} \gamma A \cos gy\, dg = \begin{cases} -(0.5jk\eta/E_0) \sum_{0}^{N} b_l \cos(l\pi y/h), & -h < y < h \\ 0, & h < |y|. \end{cases} \tag{37}$$

Multiplying both sides of (37) by $\cos g'y$ and integrating both sides over the range $0 < y < \infty$, we obtain

$$A = \frac{-jk\eta w}{\pi\gamma E_0} \sum_{0}^{N} b_l G_l \tag{38}$$

$$G_l = (1/w) \int_0^h \cos(l\pi y/h) \cos(gy)\, dy. \tag{39}$$

The boundary condition on tangential E leads to

$$\int_0^\infty A \cos gy \, dg = -1, \qquad -h < y < h. \tag{40}$$

Multiply (40) by $\cos(i\pi y/h)$ and integrate over the range $0 < y < h$ to obtain

$$\int_0^\infty A G_i \, dg = \begin{cases} -0.5, & \text{if } i = 0 \\ 0, & \text{if } i \neq 0. \end{cases} \tag{41}$$

From (38) and (41),

$$\sum_{l=0}^{N} b_l Z_{il} = V_i \tag{42}$$

$$Z_{il} = (2jk\eta w/\pi) \int_0^\infty (G_i G_l/\gamma) \, dg \tag{43}$$

where $V_i = 0$ except $V_0 \doteq E_0$.

Now let us express the current density on the strip as the sum of the edge mode and a Fourier series as in (27). Once again we obtain (30)–(32) with Z_{il} given by (43).

By integrating the current density across the strip, it is found the current is $I = wb_0 = wc_0 + wc_N$. In the broadside direction ($\phi = 0$) the scattered far-zone field is

$$E_z^s = -(k\eta I/4) \sqrt{\frac{2j}{\pi k \rho}} e^{-jk\rho}. \tag{44}$$

For normal incidence, the backscatter echo width is

$$W_e = 2\pi\rho |E^s|^2 / |E_0|^2 = \frac{k^2 \eta^2 |I|^2 \lambda}{8\pi |E_0|^2}. \tag{45}$$

VI. NUMERICAL RESULTS

Fig. 2 illustrates the reflection coefficient versus spacing for a strip grating with normal incidence. When the spacing is less than the wavelength, these data show satisfactory agreement with the measurements of Primich [10] and the formulas of Marcuvitz [11].

Fig. 3 shows the convergence properties of our calculations with (22) and (30). For numerical calculations the series in (32) is truncated after M terms, and best results are obtained if M is greater than N in (30). Good results are obtained with $M = 20$ and $N = 5$ for $0 < w/\lambda < 0.5$ or $N = 10$ for $0.5 < w/\lambda < 1$.

Accurate current distributions are not obtained when J is expressed as a Fourier series as in Section III. Suppose, for example, we choose $N = 20$ in (17) and (22). Then we find the calculated current distribution has 20 pronounced ripples across the strip. These false ripples are not observed with the edge-mode formulation in Section IV.

For a strip grating with normal incidence and spacing s less than λ, it is found the current distribution $J(y)$ has constant phase. Although the magnitude of J varies across the strip, the phase of J is precisely uniform. This is observed for all values of the strip width w. Thus $J(y)$ qualifies as a "characteristic mode" [8], [9] of the grating, since this

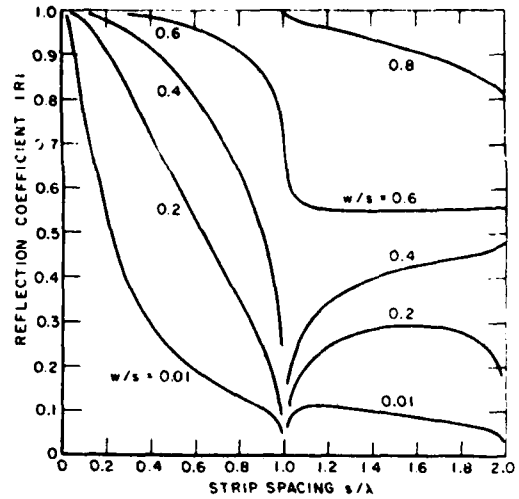

Fig. 2. Reflection coefficient of perfectly conducting strip grating with normal incidence.

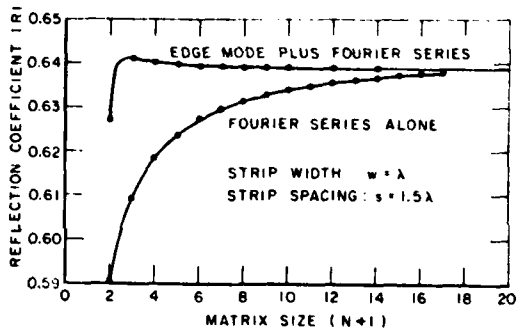

Fig. 3. Convergence curve for reflection coefficient of strip grating with normal incidence.

current distribution generates an electric field which also has constant phase across the strip. When the spacing exceeds λ, the phase of J is no longer constant.

When the strip width is just slightly smaller than the spacing, it is found the calculated current density J approaches the physical optics approximation $J = 2H^i$. With the edge mode formulation of Section IV, good results are obtained even with large spacing such as $s = 20\lambda$ or $s = 50\lambda$. When the spacing is large, the calculated reflection coefficient agrees closely with the physical optics approximation $R = w/s$.

Fig. 4 illustrates the backscatter echo width of a single strip with broadside incidence. The moment method (Section V) shows excellent agreement with the rigorous solution. Fig. 5 shows the convergence properties of our calculations.

Macrakis [12] presents the rigorous solution for the strip in terms of Mathieu functions. We used the Mathieu subroutines of Hodge [13] to tabulate the rigorous data in Fig. 4 and Table I. Our rigorous data agree with those of Macrakis in the range $0.318 < w/\lambda < 0.955$ where tabulated Mathieu functions were available to him. However, our data differ greatly from his (and from the "exact" data of King and Wu [14]) in the region $w/\lambda < 0.2$. For narrow strips with $w/\lambda < 0.1$, our data agree with calculations based on the equivalent round wire with radius $a = w/4$ (rather than $a = w/2$ as used in [12] and [14]).

With entire basis functions, convergence greatly improves

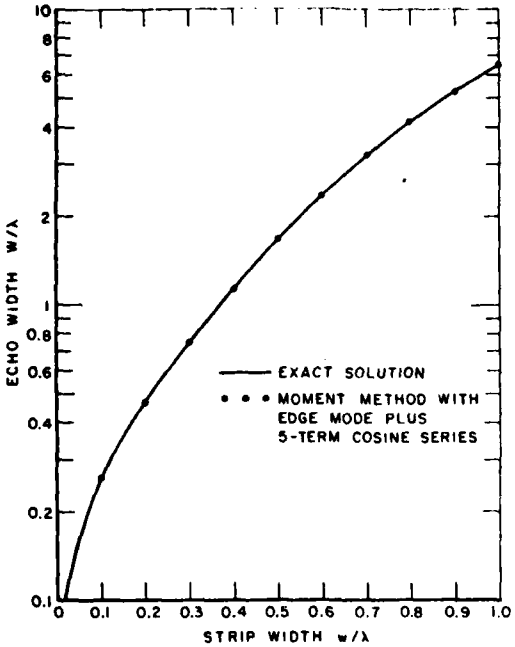

Fig. 4. Broadside backscatter echo width of perfectly conducting strip.

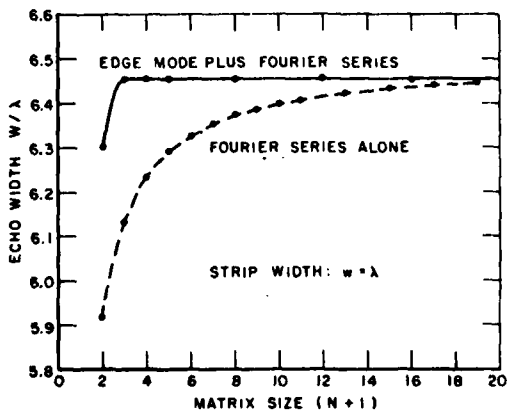

Fig. 5. Convergence curve for broadside backscatter from perfectly conducting strip.

TABLE I
BROADSIDE-BACKSCATTER ECHO WIDTH OF PERFECTLY CONDUCTING STRIP (RIGOROUS SOLUTION)

w/λ	W_e/λ	w/λ	W_e/λ
0.01	0.07593	0.1	0.26049
.02	.10315	.2	.46718
.03	.12600	.3	.74619
.04	.14687	.4	1.14024
.05	.16664	.5	1.67973
.06	.18579	.6	2.37586
.07	.20458	.7	3.22102
.08	.22321	.8	4.19756
.09	.24181	.9	5.28889
.10	.26049	1.0	6.48630

when the edge mode is included among the basis functions. It remains to be seen whether similar improvement can be obtained with subsectional bases or with three-dimensional scattering geometries such as the rectangular plate.

REFERENCES

[1] T. Larsen, "A survey of the theory of wire grids," *IEEE Trans. Microwave Theory Tech.*, vol. MTT-10, pp. 191–201, 1962.

[2] H. A. Corriher, Jr. and B. O. Pyron, "A bibliography of articles on radar reflectivity and related subjects: 1957–1964," *Proc. IEEE*, vol. 53, pp. 1025–1064, Aug. 1965.

[3] J. J. Bowman, T. B. A. Senior, and P. L. E. Uslenghi, *Electromagnetic and Acoustic Scattering by Simple Shapes*. Amsterdam: North-Holland, 1969, pp. 181–239.

[4] J. C. Minor and D. M. Bolle, "Modes in the shielded microstrip on a ferrite substrate transversely magnetized in the plane of the substrate," *IEEE Trans. Microwave Theory Tech.*, vol. MTT-19, pp. 570–577, 1971.

[5] L. Shafai and Y. S. El-Moazzen, "Radiation patterns of an antenna near a conducting strip," *IEEE Trans. Antennas Propagat.*, vol. AP-20, pp. 642–644, Sept. 1972.

[6] L. L. Tsai, D. R. Wilton, M. G. Harrison, and E. H. Wright, "A comparison of geometrical theory of diffraction and integral equation formulation for analysis of reflector antennas," *IEEE Trans. Antennas Propagat.*, vol. AP-20, pp. 705–712, Nov. 1972.

[7] D. R. Wilton and S. Govind, "Incorporation of edge conditions in moment method solutions," *IEEE Trans. Antennas Propagat.*, vol. AP-25, pp. 845–850, Nov. 1977.

[8] R. J. Garbacz, "Modal expansions for resonance scattering phenomena," *Proc. IEEE*, vol. 53, pp. 856–864, Aug. 1965.

[9] R. F. Harrington and J. R. Mautz, "Theory of characteristic modes for conducting bodies," *IEEE Trans. Antennas Propagat.*, vol. AP-19, pp. 622–628, Sept. 1971.

[10] R. I. Primich, "Some electromagnetic transmission and reflection properties of a strip grating," *IEEE Trans. Antennas Propagat.*, vol. AP-5, pp. 176–182, Apr. 1957.

[11] N. Marcuvitz, *Waveguide Handbook*. New York: McGraw-Hill, 1951, pp. 280–289.

[12] M. S. Macrakis, "Theoretical and experimental study of the backscattering cross section of an infinite ribbon," *J. Appl. Phys.*, vol. 31, pp. 2261–2266, Dec. 1960.

[13] D. B. Hodge, "The calculation of the eigenvalues and eigenfunctions of mathieu's equation," Ohio State Univ. ElectroScience Lab., Dep. Elec. Eng. Rep. 2902-4, June 1971, prepared under Grant NGL 36-008-138 for National Aeronautics and Space Administration (N72-15558).

[14] R. W. P. King and T. T. Wu, *The Scattering and Diffraction of Waves*. Cambridge, MA: Harvard Univ. Press, 1959, pp. 122–123.

[15] A. R. Neureuther and K. Zaki, "Numerical solutions of electromagnetic boundary value problems by means of the asymptotic anticipation method," *Radio Sci.*, vol. 3, pp. 1158–1167, Dec. 1968.

[16] D. A. Hill and J. R. Wait, "Electromagnetic scattering of an arbitrary plane wave by a wire mesh with bonded junctions," *Can. J. Phys.*, vol. 54, pp. 353–361, 1976.

Jack H. Richmond (S'49–M'56–SM'59–F'80) was born in Kalispell, MT on July 30, 1922. He received the B.S. degree, summa cum laude, from Lafayette College, Easton, PA, and the M.Sc. and Ph.D. degrees in electrical engineering from Ohio State University, Columbus, in 1950, 1952, and 1955, respectively.

From 1940 to 1946 and from 1950 to 1951 he served in the U.S. Navy as Chief Electronics Technician. Since 1952 he has been engaged in research on antennas and scattering at the ElectroScience Laboratory, Ohio State University. Now a Professor, he has been on the faculty of the Department of Electrical Engineering since 1955.

Dr. Richmond is a member of Tau Beta Pi, Phi Beta Kappa, Sigma Xi, Pi Mu Epsilon, and Eta Kappa Nu.

APPENDIX C

ON THE EDGE MODE IN THE THEORY OF THICK CYLINDRICAL MONOPOLE ANTENNAS

On the Edge Mode in the Theory of Thick Cylindrical Monopole Antennas

JACK H. RICHMOND, FELLOW, IEEE

Abstract—**The Fourier transform is employed to develop the theory of thick cylindrical monopole antennas. The tubular monopole with an open end is considered as well as the solid monopole with a flat end. The unknown current or field distribution is expanded in a Fourier series, and Galerkin's method is employed to develop simultaneous equations for the Fourier coefficients. When the edge mode is included among the basis functions, it is found this greatly improves the convergence of the moment-method calculations. Numerical data are included, showing excellent agreement with experimental measurements of the monopole admittance.**

I. INTRODUCTION

Einarsson [1] presents solutions for tubular and solid cylindrical-wire antennas. These solutions are based on a delta-gap model of the generator and thus are not suitable for calculating the susceptance. This objection applies also to the formulations of Chang [2] and King and Wu [3]. Otto [4] employs a realistic magnetic-frill model for the generator and reduces Einarsson's formulation to one equation with one unknown (rather than eight simultaneous equations). It has not been demonstrated that Otto's approximations are applicable to electrically thick antennas, however.

Chang [5] presents a moment-method solution for the thick tubular monopole based on Hallen's integral equation with an extra term corresponding to a radially extended source in the aperture of the coaxial feed cable. Thus an excellent solution is available for the thick tubular antenna, but evidently not for the thick solid cylindrical antenna.

King [11] presents measured admittances of thick monopoles, theoretical results for thick tubular monopoles, and a correction term for higher order modes in the coaxial feed line.

In this communication we present moment-method solutions for tubular and solid cylindrical antennas. In comparison with previous formulations, ours are straightforward. It is demonstrated that the convergence of the solution is greatly improved when the edge mode is included among the basis

Manuscript received January 3, 1980; revised April 29, 1980. This work was supported in part by Contract DAAG29-79-C-0082 between the Army Research Office and the Ohio State University Research Foundation.

The author is with the ElectroScience Laboratory, Department of Electrical Engineering, the Ohio State University, Columbus, OH 43212.

0018-926X/80/1100-0916$00.75 © 1980 IEEE

functions. Numerical results are included, showing excellent agreement between the calculated and measured admittances.

A periodic collinear array of cylindrical wires is considered briefly. When the incident field is independent of the coordinates ϕ and z, an interesting property is observed. For all values of the wire radius a, the wire length L and the spacing s (with $s < \lambda$), the induced current distribution $I(z)$ has precisely constant phase (i.e., the phase is independent of z). The electric field generated by this current also has constant phase over the cylindrical surface. Thus the solution qualifies as a "characteristic mode" as defined by Garbacz [6] and Harrington and Mautz [7]. When the spacing s exceeds λ, this constant-phase property is lost.

II. THE CENTER-FED TUBULAR DIPOLE

Fig. 1 illustrates a center-fed tubular dipole antenna. This dipole is equivalent to a monopole antenna fed via a coaxial cable through a large ground plane. The tube has perfect conductivity and infinitesimal wall thickness, and the time dependence $e^{j\omega t}$ is understood for the electromagnetic field. The field is the sum of the incident field (E^i, H^i) from the magnetic frill and the scattered field from the electric surface current on the tube. The field is independent of the angular coordinate ϕ, and the only nonzero field components are E_ρ, E_z, and H_ϕ. The scattered field may be expressed as follows:

$$H_\phi{}^s = (jk/\eta) \int_0^\infty A K_0(\gamma a) I_1(\gamma\rho) \cos(gz)\, dg, \quad \rho < a \tag{1}$$

$$H_\phi{}^s = -(jk/\eta) \int_0^\infty A I_0(\gamma a) K_1(\gamma\rho) \cos(gz)\, dg, \quad a < \rho \tag{2}$$

$$\gamma^2 = g^2 - k^2 \tag{3}$$

where $k = \omega\sqrt{\mu\epsilon}$, $\eta = \sqrt{\mu/\epsilon}$, I_n and K_n are the modified Bessel functions, A is a function of g, and (ρ, ϕ, z) denote the coordinates in the circular cylindrical system. Except for the conducting tube, the medium is homogeneous with parameters μ and ϵ. The scattered field component $E_z{}^s$ is continuous across the boundary at $\rho = a$. Setting $E_z(a, z) = 0$ on the perfectly conducting tube, we obtain the integral equation for the tubular dipole:

$$\int_0^\infty \gamma A I_0(\gamma a) K_0(\gamma a) \cos(gz)\, dg = -E_z{}^i(a, z), \quad -h < z < h. \tag{4}$$

We multiply both sides of (4) by $\cos(i\pi z/L)$ and integrate over the region $0 < z < h$ to obtain:

$$\int_0^\infty \gamma A I_0(\gamma a) K_0(\gamma a) G_i\, dg = -V_i \tag{5}$$

$$G_i = \int_0^h \cos(gz) \cos(i\pi z/L)\, dz \tag{6}$$

$$V_i = \int_0^h E_z{}^i(a, z) \cos(i\pi z/L)\, dz \tag{7}$$

where $L = 2h$.

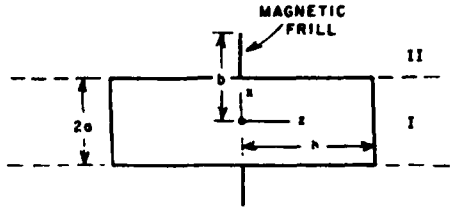

Fig. 1. Center-fed cylindrical antenna.

It is convenient to express the current distribution on the antenna in a Fourier series as follows:

$$I(z) = \sum_l b_l \cos(l\pi z/L) \tag{8}$$

where l is a positive odd integer. The scattered field must satisfy the boundary condition

$$H_\phi{}^s(a+, z) - H_\phi{}^s(a-, z) = J_s(z) \tag{9}$$

$$J_s(z) = \begin{cases} I(z)/(2\pi a), & -h < z < h \\ 0, & h < z < \infty \end{cases} \tag{10}$$

where J_s denotes the sum of the electric surface-current densities J_z on the inner and outer surfaces of the tube. From (1), (2), and (9),

$$\frac{k}{j\eta a} \int_0^\infty (A/\gamma) \cos(gz)\, dg = J_s(z). \tag{11}$$

We multiply both sides of (11) by $\cos(g'z)$ and integrate over the region $0 < z < \infty$ to obtain

$$A = \frac{j\eta\gamma}{\pi^2 k} \sum_l b_l G_l. \tag{12}$$

In (5) let us replace A with the equivalent quantity from (12). This leads to the following system of simultaneous linear equations:

$$\sum_{l=1}^{N} b_l Z_{il} = V_i, \qquad i = 1, 3, 5, \cdots, N \tag{13}$$

$$Z_{il} = \frac{-j\eta}{\pi^2 k} \int_0^\infty \gamma^2 I_0(\gamma a) K_0(\gamma a) G_i G_l\, dg. \tag{14}$$

The impedance matrix Z_{il} is symmetric. The current distribution represented by (8) is a periodic even function with period $4h$. Since each term vanishes when $z = h$, (8) represents a current distribution which vanishes at each end of the tubular dipole.

Corresponding to the TEM mode in the coaxial feed cable, let the frill in Fig. 1 have the following magnetic surface-current density:

$$M_z = \frac{-\phi V_{11}}{\rho \ln(b/a)} \tag{15}$$

where V_{11} denotes the generator voltage and b is the outer

radius of the coaxial cable. For $\rho < a$, the free space field of the magnetic frill is [8]

$$H_\phi{}^i = \frac{jkV_{11}}{\pi\eta \ln(b/a)} \int_0^\infty (1/\gamma)[K_0(\gamma a) - K_0(\gamma b)] \cdot I_1(\gamma\rho)\cos(gz)\,dg. \tag{16}$$

From (7) and (16), the excitation voltages for the center-fed tubular dipole are

$$V_i = \frac{V_{11}}{\pi \ln(b/a)} \int_0^\infty [K_0(\gamma a) - K_0(\gamma b)] I_0(\gamma a)\, G_i\, dg. \tag{17}$$

The admittance of the tubular dipole is determined as follows:

$$Y_{11} = I(0)/V_{11} = (1/V_{11}) \sum_l b_l. \tag{18}$$

Now consider the scattering problem where a plane wave has broadside incidence on the conducting tube. The incident field is

$$E_z{}^i = E_0 e^{-jkx} \approx E_0 J_0(k\rho). \tag{19}$$

From (7) and (19), the excitation voltages are

$$V_i = (-1)^n \frac{2h}{i\pi} E_0 J_0(ka) \tag{20}$$

where $n = (i-1)/2$. Of course, if the cylinder has a large radius, the higher order modes with $\cos(m\phi)$ behavior cannot be neglected.

Finally, let us consider a periodic collinear array of tubular dipoles. As in Fig. 2, let s denote the center-to-center spacing. Equations (7), (8), and (13) apply, and

$$Z_{il} = \frac{-j\eta}{\pi k s} \sum_{n=0}^{\infty} e_n \gamma_n{}^2 I_0(\gamma_n a) K_0(\gamma_n a) G_{in} G_{ln} \tag{21}$$

$$\gamma_n{}^2 = (2n\pi/s)^2 - k^2 \tag{22}$$

$$G_{ln} = \int_0^h \cos(l\pi z/L)\cos(2n\pi z/s)\,dz \tag{23}$$

where $e_n = 2$ except $e_0 = 1$. When a plane wave has broadside incidence on the array, the voltages V_i are given by (20). Equations (13) and (20)–(23) were programmed for the digital computer. When the spacing s is less than or equal to λ, it is found the complex Fourier coefficients b_l all have the same phase angle. It follows from (8) that the phase of $I(z)$ is independent of z.

III. EDGE MODE FOR THE TUBULAR DIPOLE

Let us express the current distribution on the tubular dipole as the sum of an edge mode, a feed mode, and a Fourier series, as follows:

$$I(z) = I_e(z) + I_f(z) + \sum_l c_l \cos(l\pi z/L). \tag{24}$$

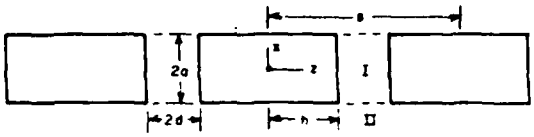

Fig. 2 Periodic collinear array of cylinders

The idea is to separate out the rapidly varying components of the current distribution. Then the Fourier series may converge rapidly since it represents a smooth function. With the moment method, one must invert the impedance matrix Z_{il} to determine the Fourier coefficients and the antenna admittance. Thus any technique that reduces the size of the matrix Z_{il} implies a reduction in computational expense and storage requirements and the capability of solving longer dipole antennas.

In the vicinity of each end of the tubular dipole, it is known that $I(z)$ must behave like the square root of the distance from the end [9]. Thus a suitable edge mode is

$$I_e(z) = c_N\sqrt{1-(z/h)^2} = c_N \sum_l d_l \cos(l\pi z/L) \tag{25}$$

$$d_l = (2/l)J_1(l\pi/2) \tag{26}$$

where J_1 denotes the Bessel function. There is only one unknown constant c_N in the edge mode.

The current function $I(z)$ often has large slope in the vicinity of the feedpoint, which in the present case is at the center of the dipole. This component of $I(z)$ is the same as the current distribution $I_0(z)$ on an infinitely long cylindrical antenna. Thus a suitable feed mode is

$$I_f(z) = I_0(z)\cos(\pi z/L) = \sum_l f_l \cos(l\pi z/L). \tag{27}$$

The factor $\cos(\pi z/L)$ is included so the feed mode, like all the other modes in (24), will vanish at the ends of the dipole. The current distribution on the infinitely long cylinder with magnetic-frill excitation is [8]:

$$I_0(z) = \frac{2jkV_{11}}{\eta \ln(b/a)} \int_0^\infty \frac{[K_0(\gamma a) - K_0(\gamma b)]\cos(gz)\,dg}{\gamma^2 K_0(\gamma a)}. \tag{28}$$

An efficient subroutine is available for calculating the function $I_0(z)$. The Fourier coefficients f_l for the feed mode are calculated via numerical integration. The feed mode contains no unknown constants.

From (8), (24), (25), and (27),

$$b_l = c_l + c_N d_l + f_l. \tag{29}$$

In (13) we replace b_l with the equivalent quantity from (29) to obtain the following system of simultaneous linear equations:

$$\sum_{l=1}^{N} c_l Z_{il}' = V_i', \qquad i = 1, 3, \cdots, N \tag{30}$$

$$V_i' = V_i - \sum_{l=1}^{\infty} f_l Z_{il} \tag{31}$$

$$Z_{il}' = Z_{il}, \qquad l < N \tag{32}$$

$$Z_{iN}' = \sum_{l=1}^{\infty} d_l Z_{il} \tag{33}$$

where V_i and Z_{il} are given by (14) and (17). As N is increased, the admittance converges much more rapidly with (30) than with (13). The impedance matrix Z_{il}' is not symmetric. Although most of the constants c_l are Fourier coefficients, the last one c_N represents the amplitude of the edge mode. The quantities d_l and f_l are known constants.

In the plane wave scattering problem, it is better to delete the feed mode. In this case, V_i and V_i' are given by (20).

IV. PERIODIC COLLINEAR ARRAY OF SOLID DIPOLES

Let us consider a periodic collinear array of solid perfectly conducting cylindrical dipoles with flat ends, as shown in Fig. 2. The incident field (E^i, H^i) is considered to be periodic also with period s, and the source is located in the exterior region where $\rho > a$. The field may be expressed as follows:

$$H_\phi = (jk/\eta) \sum_{l=0}^{\infty} \frac{B_l I_1(\gamma_l \rho)}{\gamma_l I_0(\gamma_l a)} \cos(l\pi z'/d), \qquad \rho < a \tag{34}$$

$$H_\phi = H_\phi^i - (jk/\eta) \sum_{n=0}^{\infty} \frac{A_n K_1(\gamma_n \rho)}{K_0(\gamma_n a)} \cos(2n\pi z/s), \qquad \rho > a \tag{35}$$

$$H_\phi^i = (jk/\eta) \sum_n E_n I_1(\gamma_n \rho) \cos(2n\pi z/s), \qquad \rho \leq a \tag{36}$$

where $z' = z - h$. It is easy to verify that (34) represents a field with E_ρ vanishing over the flat ends of the cylinders at $z' = 0$ and $z' = 2d$. Equation (34) is valid only in region I where $h < z < h + 2d$. Of course, the field vanishes in the interior of each solid cylinder.

The field $E_z(a+, z)$ must vanish on the surface of the conducting cylinders, and it must match $E_z(a-, z)$ over the aperture between cylinders. Thus

$$A_n = \frac{2e_n}{\gamma_n s} \sum_l B_l F_{ln} - I_0(\gamma_n a) E_n \tag{37}$$

$$F_{ln} = \int_0^d \cos(l\pi z'/d) \cos(2n\pi z/s)\, dz'. \tag{38}$$

The field $H_\phi(a+, z)$ must match the field $H_\phi(a-, z)$ over the aperture. This leads to

$$\sum_n \frac{A_n K_1(\gamma_n a) F_{in}}{K_0(\gamma_n a)} = \sum_n E_n I_1(\gamma_n a) F_{in} - \frac{dB_i I_1(\gamma_i a)}{e_i \gamma_i I_0(\gamma_i a)}. \tag{39}$$

From (37) and (39) we obtain the simultaneous linear equations:

$$\sum_{l=0}^{N} B_l Z_{il} = V_i, \qquad i = 0, 1, \cdots, N \tag{40}$$

$$V_i = jk \sum_n \frac{E_n F_{in}}{\gamma_n a K_0(\gamma_n a)} \tag{41}$$

$$Z_{il} = \frac{jkdI_1(\gamma_i a)\delta_{il}}{e_i \gamma_i I_0(\gamma_i a)} + (2jk/s) \sum_n \frac{e_n K_1(\gamma_n a) F_{in} F_{ln}}{\gamma_n K_0(\gamma_n a)}. \tag{42}$$

As usual, we assume the incident field (and the Fourier coefficients E_n) is known. The B_l are determined from (40) by matrix inversion or equivalent techniques. Then the A_n are obtained from (37). Although the details cannot be presented here, one can then determine the current distribution and the admittance of the solid cylindrical antenna. The aperture field can be expressed as the sum of an edge mode plus a well-behaved residue with techniques analogous to those presented for the tubular cylinder.

V. NUMERICAL RESULTS

Let us discuss first the numerical results for the tubular antenna. Fig. 3 illustrates the convergence curves for the admittance of a tubular dipole. M denotes the size of the matrix Z_{il} (i.e., the number of simultaneous linear equations) in the moment-method calculations. A dramatic improvement is to be noted in Fig. 3 when the current distribution is represented as the sum of the edge mode, the feed mode, and a Fourier series. Convergence is obtained with $M = 6$, whereas M must exceed 40 when the current is represented by a Fourier series alone.

Fig. 4 illustrates the admittance versus length for a tubular monopole. Our calculations show excellent agreement with the experimental measurements of Holly [10]. In these calculations accuracy was more important than computational economy. Therefore, we used $M = 10$ for Fig. 4. In the infinite

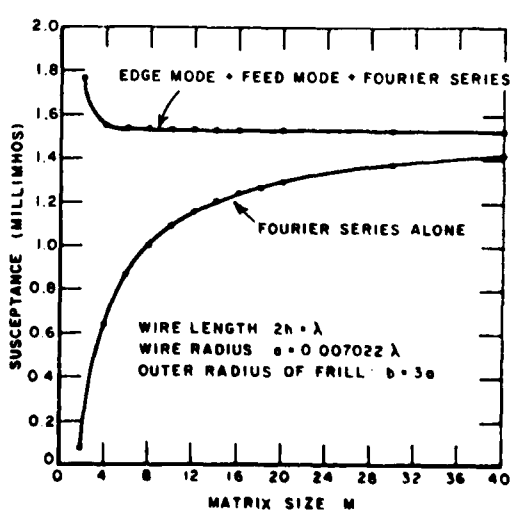

Fig. 3. Convergence curve for susceptance of center-fed tubular dipole.

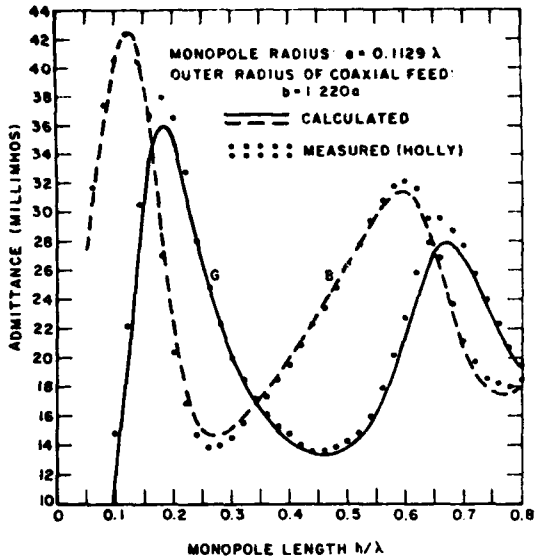

Fig. 4. Admittance of tubular monopole with open end.

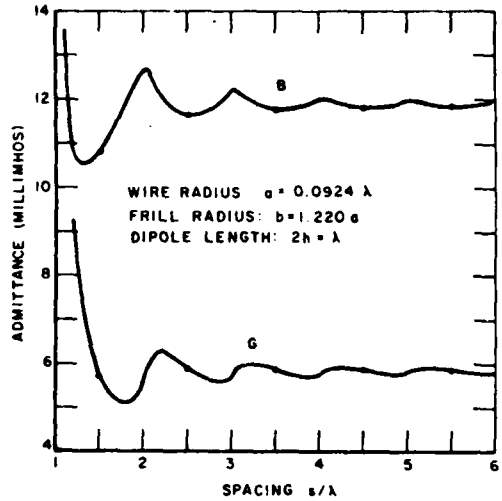

Fig. 6. Admittance versus spacing for periodic collinear array of solid center-fed cylindrical antennas with flat ends.

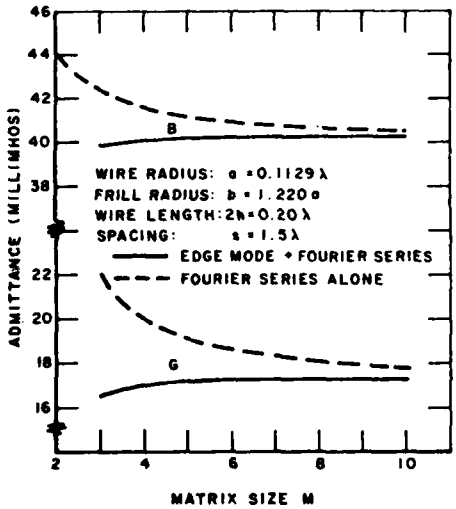

Fig. 5. Convergence curve for admittance of solid center-fed cylindrical antenna with flat ends.

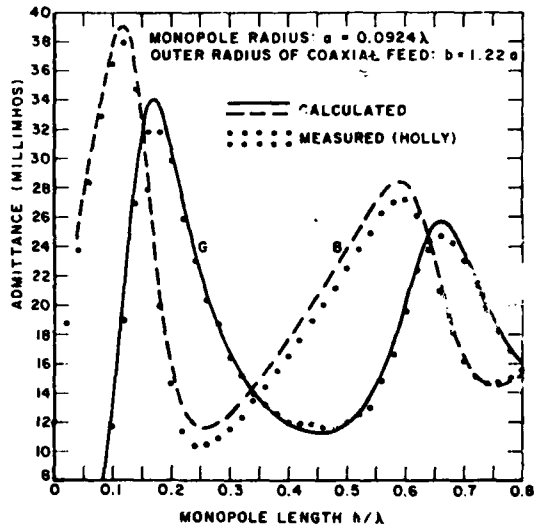

Fig. 7. Admittance of solid cylindrical monopole with flat end.

series in (31) and (33), let LL denote the number of terms actually summed. We used $LL = 20$ for Fig. 4.

For the solid cylindrical antenna, Fig. 5 shows substantial improvement in convergence when the edge mode is included among the basis functions. Fig. 6 illustrates the admittance versus spacing for a periodic collinear array of solid dipoles. Usually, one is interested in a single dipole rather than an array. The admittance converges rapidly with K if $s/\lambda = K + 1/2$ where K denotes an integer. Thus the array admittance is essentially equal to the single-dipole admittance when $s/\lambda = 3.5$ in Fig. 6.

Fig. 7 illustrates the admittance versus length for a solid cylindrical monopole. Again, the calculations show excellent agreement with experimental measurements. In these calculations we used $M = 14$ and $LL = 20$. In the calculations for Fig. 7 we let $s/\lambda = 5.5$.

REFERENCES

[1] O. Einarsson, "A comparison between tube-shaped and solid cylinder antennas," *IEEE Trans. Antennas Propagat.*, vol. AP-14, pp. 31-37, Jan. 1966.

[2] D. C. Chang, "On the electrically thick cylindrical antenna," *Radio Sci.*, vol. 2, pp. 1043-1060, Sept. 1967.

[3] R. W. P. King and T. T. Wu, "The thick tubular transmitting antenna," *Radio Sci.*, vol. 2, pp. 1061-1065, Sept. 1967.

[4] D. V. Otto, "Fourier transform method in cylindrical antenna theory," *Radio Sci.*, vol. 3, pp. 1050-1057, Nov. 1968.

[5] D. C. Chang, "On the electrically thick monopole, part I: Theoretical solution," *IEEE Trans. Antennas Propagat.*, vol. AP-16, pp. 58-64, Jan. 1968.

[6] R. J. Garbacz, "Modal expansions for resonance scattering phenomena," *Proc. IEEE*, vol. 53, pp. 856-864, Aug. 1965.

[7] R. F. Harrington and J. R. Mautz, "Theory of characteristic modes for conducting bodies," *IEEE Trans. Antennas Propagat.*, vol. AP-19, pp. 622-628, Sept. 1971.

[8] J. H. Richmond, "Admittance of infinitely long cylindrical wire with finite conductivity and magnetic frill excitation," *IEEE Trans. Antennas Propagat.*, vol. AP-27, pp. 264-266, Mar. 1979.

[9] J. Van Bladel, *Electromagnetic Fields*. New York: McGraw-Hill, 1964, pp. 382-387.

[10] S. Holly, "Experimental study of electrically thick monopole antennas," Cruft Lab., Harvard Univ., Cambridge, MA, Sci. Rep. 8, Dec. 1969.

[11] R. W. P. King, "Measured admittances of electrically thick monopoles," *IEEE Trans. Antennas Propagat.*, vol. AP-20, pp. 763-766, Nov. 1972.

evaluate the current are given. The transient current induced on the wire is compared to the current computed by assuming quasi-steady-state theory.

The interpretations and restrictions of all the given solutions are discussed.

APPENDIX D

FIELD OF SEPARABLE ELECTRIC SOURCE CURRENT DISTRIBUTION IN FREE SPACE

Radio Science, Volume 16, Number 6, pages 1299–1301, November–December 1981

Field of separable electric source current distribution in free space

Jack H. Richmond

The Ohio State University ElectroScience Laboratory, Department of Electrical Engineering, Columbus, Ohio 43212

(Received February 19, 1981; revised May 19, 1981; accepted May 19, 1981.)

Simple rigorous expressions are developed for the fields of an electric source current distribution that is separable in cartesian coordinates. The medium is unbounded free space, and the time-harmonic source current exists in the slab region $z_1 < z < z_2$.

INTRODUCTION

Many textbooks present the theory of separable fields in a source-free homogeneous region. However, they do not relate these fields to the sources or determine the fields in the source region. These relations and expressions are useful, for example, in the study of propagation in periodic media, radiation from a periodic array of sources, and scattering from a periodic array of metallic or dielectric elements.

THEORY

Consider a time-harmonic electric current density with the form

$$\mathbf{J} = (\hat{x}A + \hat{y}B + \hat{z}C)\,X(x)\,Y(y)\,F(z) \tag{1}$$

where A, B, and C are arbitrary constants, the time dependence $e^{j\omega t}$ is suppressed, $F(z)$ is an arbitrary function, and

$$X'' = \gamma_1^2 X \tag{2}$$

$$Y'' = \gamma_2^2 Y \tag{3}$$

Primes denote derivatives, and γ_1 and γ_2 are arbitrary complex constants. Suitable functions are

$$X(x) = \cosh \gamma_1 x,\ \sinh \gamma_1 x,\ e^{\gamma_1 x},\ e^{-\gamma_1 x} \tag{4}$$

$$Y(y) = \cosh \gamma_2 y,\ \sinh \gamma_2 y,\ e^{\gamma_2 y},\ e^{-\gamma_2 y} \tag{5}$$

or linear combinations of these functions.

Let the source $\mathbf{J}$ exist only in the slab region $z_1 < z < z_2$. If the medium everywhere is free space, the vector potential is given as follows:

$$\mathbf{A}(x, y, z) = \iiint \mathbf{J}(x', y', z')\,\frac{e^{-jkR}}{4\pi R}\,dx'\,dy'\,dz' \tag{6}$$

If X and Y satisfy (2) and (3), it is shown in Appendix 1 that

$$\iint_{-\infty}^{\infty} X(x')\,Y(y')\,\frac{e^{-jkR}}{R}\,dx'\,dy' = (2\pi/\gamma_3)\,X(x)\,Y(y)\,e^{-\gamma_3|z-z'|} \tag{7}$$

$$\gamma_1^2 + \gamma_2^2 + \gamma_3^2 = -k^2 = -\omega^2\mu\varepsilon \tag{8}$$

From (6)–(7), the vector potential is

$$\mathbf{A} = (\hat{x}A + \hat{y}B + \hat{z}C)\,XYZ/(2\gamma_3) \tag{9}$$

$$Z(z) = \int_{z_1}^{z_2} F(z')\,e^{-\gamma_3|z-z'|}\,dz' = Pe^{-\gamma_3 z} + Qe^{\gamma_3 z} \tag{10}$$

$$P = \begin{cases} 0 & z < z_1 \\ \displaystyle\int_{z_1}^{z} F(z')\,e^{\gamma_3 z'}\,dz' & z_1 < z < z_2 \\ \displaystyle\int_{z_1}^{z_2} F(z')\,e^{\gamma_3 z'}\,dz' & z_2 < z \end{cases} \tag{11}$$

$$Q = \begin{cases} 0 & z_2 < z \\ \displaystyle\int_{z}^{z_2} F(z')\,e^{-\gamma_3 z'}\,dz' & z_1 < z < z_2 \\ \displaystyle\int_{z_1}^{z_2} F(z')\,e^{-\gamma_3 z'}\,dz' & z < z_1 \end{cases} \tag{12}$$

$$Z'' = \gamma_3^2 Z - 2\gamma_3 F \tag{13}$$

The magnetic field intensity is found as follows:

Copyright © 1981 by the American Geophysical Union.

Paper number 1S0914.
0048-6604/81/1112-0914$01.00

$$\mathbf{H} = \nabla \times \mathbf{A} \tag{14}$$

$$H_x = (CXY'Z - BXYZ')/(2\gamma_3) \tag{15}$$

$$H_y = (AXYZ' - CX'YZ)/(2\gamma_3) \tag{16}$$

$$H_z = (BX'YZ - AXY'Z)/(2\gamma_3) \tag{17}$$

The electric field intensity is given by

$$\mathbf{E} = (\nabla \times \mathbf{H} - \mathbf{J})/(j\omega\varepsilon) \tag{18}$$

$$E_x = [(k^2 + \gamma_1^2)AXYZ + BX'Y'Z + CX'YZ']\,D \tag{19}$$

$$E_y = [AX'Y'Z + (k^2 + \gamma_2^2)BXYZ + CXY'Z']\,D \tag{20}$$

$$E_z = [AX'YZ' + BXY'Z' + (k^2 + \gamma_3^2)CXYZ - 2\gamma_3 CXYF]\,D \tag{21}$$

$$D = 1/(2j\omega\varepsilon\gamma_3) \tag{22}$$

In (21) the last term vanishes if $z < z_1$ or $z > z_2$.

With the aid of (1)–(3), (8), (9), and (13), it is easy to show that our vector potential $\mathbf{A}$ satisfies the appropriate wave equation

$$\nabla^2\mathbf{A} + k^2\mathbf{A} = -\mathbf{J} \tag{23}$$

Since our solution in (15)–(17) and (19)–(21) is derived via (14) and (18), it is not difficult to show that is satisfies all four of Maxwell's differential equations. In Appendix 2 it is shown that it also satisfies the required boundary conditions at $z = z_2$. The radiation conditions at $z \to \infty$ will be satisfied if we choose the proper root for γ_3.

Theorems are available that make it possible to use the above free-space fields even when the medium is not free space. For example, suppose one has a periodic array of perfectly conducting wires surrounded by free space. It is well known that the field will not be disturbed when the wires are removed if the surface-current density is maintained in free space. Next, suppose one has a periodic array of dielectric rods surrounded by free space. Without disturbing the field, one may remove the rods while maintaining the polarization-current density $\mathbf{J} = j\omega(\varepsilon_1 - \varepsilon)\mathbf{E}$ in free space. If the permeability μ_1 of the rods differs from μ, then the magnetic current density $\mathbf{M} = j\omega(\mu_1 - \mu)\mathbf{H}$ is required also.

Suppose one has a periodic array of wires or rods in the region $z_1 < z < z_2$ and the surrounding medium is free space. Then one may write a suitable expression for the current density $\mathbf{J}(x, y, z)$ and apply the Fourier transform with respect to the x and y variables. The resulting expression for $\mathbf{J}$ will be a summation of separable current functions. Each term will have the form of (1) with a subscript n inserted on the quantities A, B, C, X, and Y. Then the field of the periodic array is given by (15)–(21) with insertion of subscripts and summations.

CONCLUSION

Simple rigorous expressions are developed for the fields of an electric source current distribution that is separable in cartesian coordinates. The medium is unbounded free space, and the time-harmonic source current exists in the slab region $z_1 < z < z_2$.

APPENDIX 1: EVALUATION OF THE DOUBLE INTEGRAL

The double integral in (7) can be evaluated most readily with a technique presented by *Harrington* [1961]. In this method, one solves a radiation problem by two different methods and equates the two solutions. To apply this method, let us consider an infinite sheet of electric surface-current density $\mathbf{J}_s = \hat{x}X(x)Y(y)$ located on the plane surface $z = z'$ and radiating in free space, where X and Y satisfy (2) and (3). From the boundary conditions and symmetry considerations, $H_y = \pm XY/2$ when $z \to z'$. It is easy to deduce that

$$H_y = -(1/2)X(x)Y(y)\,\mathrm{sgn}\,(z - z')e^{-\gamma_3|z-z'|} \tag{24}$$

and therefore the vector potential is

$$A_x = X(x)Y(y)e^{-\gamma_3|z-z'|}/(2\gamma_3) \tag{25}$$

But the vector potential is also given by

$$A_x = \iint_{-\infty}^{\infty} X(x')Y(y')\frac{e^{-jkR}}{4\pi R}\,dx'\,dy' \tag{26}$$

By equating these two expressions for A_x, we obtain (7).

An alternative derivation of (7) is available if $\gamma_1 = jf_1$ and $\gamma_2 = jg_2$ in (2) and (3), where f_1 and g_2 are real constants. The following expansion

$$\frac{e^{-jkR}}{R} = \iint_{-\infty}^{\infty} \frac{e^{-jf(x-x')}e^{-jg(y-y')}e^{-\gamma_3|z-z'|}}{2\pi\gamma_3}\,df\,dg \tag{27}$$

$$\gamma_3^2 = f^2 + g^2 - k^2 \tag{28}$$

is developed by *Tyras* [1969]. We substitute (27) into (6), interchange the order of the integrations, and note that

$$\int_{-\infty}^{\infty} e^{j(f+f_1)x'}\,dx' = 2\pi\delta(f+f_1) \tag{29}$$

$$\int_{-\infty}^{\infty} e^{j(g+g_2)y'}\,dy' = 2\pi\delta(g+g_2) \tag{30}$$

This procedure leads again to (7) and (8).

APPENDIX 2: THE BOUNDARY CONDITIONS

In order to be correct, the solution presented in (15)–(21) must satisfy certain boundary conditions at the surfaces $z = z_1$ and $z = z_2$. For the sake of brevity, let us consider only the boundary at $z = z_2$. From (15), (16), (19), and (20), the tangential field components H_x, H_y, E_x, and E_y are continuous across this boundary if Z and Z' are continuous. We recognize these as the appropriate boundary conditions for a surface that does not contain a sheet of surface current density. From (10)–(12),

$$Z(z) = e^{-\gamma_3 z}\int_{z_1}^{z} F(z')e^{\gamma_3 z'}\,dz' + e^{\gamma_3 z}\int_{z}^{z_2} F(z')e^{-\gamma_3 z'}\,dz' \tag{31}$$

$$Z'(z) = -\gamma_3 e^{-\gamma_3 z}\int_{z_1}^{z} F(z')e^{\gamma_3 z'}\,dz' + \gamma_3 e^{\gamma_3 z}\int_{z}^{z_2} F(z')e^{-\gamma_3 z'}\,dz' \tag{32}$$

for $z_1 < z < z_2$, and

$$Z(z) = e^{-\gamma_3 z}\int_{z_1}^{z_2} F(z')e^{\gamma_3 z'}\,dz' \tag{33}$$

$$Z'(z) = -\gamma_3 e^{-\gamma_3 z}\int_{z_1}^{z_2} F(z')e^{\gamma_3 z'}\,dz' \tag{34}$$

for $z > z_2$. If the function $F(z)$ is well behaved at $z = z_2$, a study of (31)–(34) shows that Z and Z' are continuous across the boundary at $z = z_2$. Thus the tangential field components satisfy the required boundary conditions. From (17) it also follows that H_z is continuous as required in the given circumstances.

On the surface $z = z_2$, the surface charge density is

$$\rho_s = CXYF(z_2)/(j\omega) \tag{35}$$

The required boundary condition on the normal component of **E** is

$$\rho_s = \varepsilon E_z^{I}(z_2) - \varepsilon E_z^{II}(z_2) \tag{36}$$

where $z > z_2$ in region I and $z_1 < z < z_2$ in region II. In (21) for E_z, all the terms are continuous except the last one. Since $F(z)$ vanishes in region I, it is evident that our solution does satisfy (36).

Finally, let $F(z)$ consist of a unit impulse function $F(z) = \delta(z - z'')$. From (10)–(12),

$$Z(z) = e^{-\gamma_3|z-z''|} \tag{37}$$

$$Z'(z) = -\gamma_3\,\mathrm{sgn}\,(z - z'')e^{-\gamma_3|z-z''|} \tag{38}$$

Thus Z is continuous across the boundary at $z = z''$. From (15)–(22),

$$H_x^{I} - H_x^{II} = BXY \tag{39}$$

$$H_y^{I} - H_y^{II} = -AXY \tag{40}$$

$$E_x^{I} - E_x^{II} = -CX'Y/(j\omega\varepsilon) \tag{41}$$

$$E_y^{I} - E_y^{II} = -CXY'/(j\omega\varepsilon) \tag{42}$$

where $z > z''$ in region I and $z < z''$ in region II. The electric surface current density at $z = z''$ is

$$\mathbf{J}_s = (\hat{x}A + \hat{y}B)XY \tag{43}$$

From the equivalence principle of *Mayes* [1958], the electric current density J_s can be replaced with an equivalent magnetic surface current density given by

$$\mathbf{M}_s = (-\hat{x}CXY' + \hat{y}CX'Y)/(j\omega\varepsilon) \tag{44}$$

It is easy to show that (39)–(42) satisfy the required boundary conditions at the surface $z = z''$, which contains electric and magnetic surface current densities.

Acknowledgments. This work was supported in part by contract DAAG29-79-C-0082 between The Department of the Army, U.S. Army Research Office, and The Ohio State University Research Foundation.

REFERENCES

Harrington, R. F. (1961), *Time-Harmonic Electromagnetic Fields*, pp. 242–244, McGraw-Hill, New York.

Mayes, P. E. (1958), The equivalence of electric and magnetic sources, *IEEE Trans. Antennas Propag.*, *AP-6*, 295–296.

Tyras, G. (1969), *Radiation and Propagation of Electromagnetic Waves*, pp. 105–106, Academic, New York.

APPENDIX E

SCATTERING FROM CYLINDRICAL INHOMOGENEITIES IN A LOSSY MEDIUM

Radio Science, Volume 17, Number 5, pages 973–987, September–October 1982

Scattering from cylindrical inhomogeneities in a lossy medium

Leon Peters, Jr., and Jack H. Richmond

The Ohio State University ElectroScience Laboratory, Department of Electrical Engineering, Columbus, Ohio 43212

(Received September 18, 1981; revised March 23, 1982; accepted March 23, 1982.)

Many buried scattering objects of interest take the form of two-dimensional geometries. This includes scattering from utility lines, tunnels, and geological structures such as fault lines. Radar systems used to detect these objects commonly use antennas that are at least comparable in size to the depth of the target. Thus the target and the antenna do not satisfy far zone conditions, and the radar range equation is not applicable. Consequently, the usual separate analyses of range, antenna, and target are not possible. In a previous paper a method was outlined that permitted the antenna properties and the scattering properties of a two-dimensional target to be treated separately for the case of a linear electric or magnetic dipole source parallel to the axis of the two-dimensional scatterer. This involved computing the received voltage for an antenna located at the image position, i.e., at twice the target range, and computing the backscattered fields for an electric or magnetic line source at the position of the transmitting antenna. This model has also been applied approximately to a video pulse radar with an orthogonal dipole antenna system. It would also be applicable to large loop antennas quite commonly used in geophysical explorations, as will be discussed. The primary goal of this paper is to discuss additional scattering analyses that could be used to extend the previous results. The major thrust then is to generate solutions for the scattering attenuation function (SAF), which has the form E^s/E^I or H^s/H^I where the E^I (or H^I) are the electric (or magnetic) fields of an electric (or magnetic) line source at the image position and the E^s (or H^s) are the respective scattered fields. Eigenfunction solutions have been used to obtain the SAF for circular cylindrical geometries to represent pipes and tunnels. Moment method solutions have been applied to perfectly conducting wires with and without a dielectric sheath. Moment method solutions have been applied to noncircular penetrable bodies using the polarization currents to represent the unknowns. Such solutions were developed for a line source above dikes by Parry and Ward (1971) and Hohman (1975) in the early seventies. Such solutions can be made for frequencies that include several target resonances for potential target identification. These solutions can possibly be extended to include fault lines, joints, etc., provided their electrical properties can be estimated by using some of the concepts involved in the hybrid geometrical theory of diffraction–moment approach. The methods of the modified geometrical optics could also be applied to obtain scattered fields at higher frequencies. These and other potential approaches will be discussed.

INTRODUCTION

Scattering from buried objects differs from that in free space in several significant respects. First, there is automatically a two-layer geometry since an earth–free space interface is present with the probes being located at the interface or in free space. This can be accounted for when the radiators are infinite line sources or infinitesimal electric or magnetic (small loops) dipoles. However, the analysis becomes more complex for finite antenna geometries and generally involves substantial computation time. In this paper we consider only the scattering from lossy objects immersed in lossy homogeneous media.

Copyright 1982 by the American Geophysical Union.

Paper number 2S0487.
0048-6604/82/0910-0487$08.00

Actually, *Parry and Ward* [1971] partially remove the half space in part of their analyses of the scattering from dikes. They included the half space in the field incident on the dike but not in the fields scattered from the dike. Comparison with the solution when the half space is completely included gave variations of the order of 10%. This, of course, is trivial in comparison to variations in geometry for 'real world' situations.

Second, losses in the ambient medium occur as the wave propagates through the medium and over the target.

Third, many targets which are to be detected using a three-dimensional antenna system are in essence two-dimensional, e.g., utility lines, tunnels, faults, and joints. Consequently, it becomes impractical to describe the target in terms of far field concepts such as

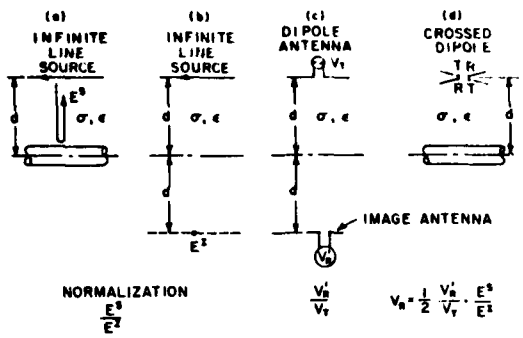

Fig. 1. Introducing the scattering attenuation function of a cylinder into the radar model.

echo area (or radar cross section) or echo width. One definition that partially alleviates this difficult is that of the scattering attenuation function (SAF) [*Burrell et al.*, 1979]. This parameter will be defined in the next section. It reduces the scattering problem to that of a line source in the vicinity of the two-dimensional target.

Ward [1980] has summarized the significant developments of electromagnetic scattering analysis as it pertains to the lossy earth. In his notation, the approach used herein reduces the three-dimensional source two-dimensional inhomogeneity to a two-dimensional source two-dimensional inhomogeneity.

Stoyer and Greenfield [1976] have previously considered the three-dimensional source two-dimensional target geometry in the presence of an interface. However, they used a point (infinitesimal) source and Fourier transform techniques. The approach to be introduced here makes it possible to use a finite length source.

Pridmore [1978] also worked the three-dimensional source three-dimensional target configuration. *Richmond* [1978] has treated this problem where the three-dimensional source was an infinitesimal magnetic dipole and the three-dimensional target was a conducting sphere as modeled by a wire grid. Actually, the wire configuration could be arranged to fit any conducting shape. It is observed that most analytic results obtained to date in the geophysical literature are for scatterers in the so-called Rayleigh region, i.e., below resonance, whereas the results discussed herein include the resonance region.

Most of the work at the ElectroScience Laboratory has been directed toward physically small targets nearer the surface at higher frequencies. The medium in this case is a lossy dielectric in contrast to the conducting medium used throughout the geophysical literature. Further, many of the targets of interest are hollow cylinders, e.g., plastic pipes and tunnels. Thus one must be cautious in extending all of these results to the low-frequency conducting media. Nevertheless, if one uses such parameters as index of refraction and impedance, then this difficulty should be averted. There is one other significant advantage to working with shallower targets; that is the ability to be able to measure the scattered fields and to compare them with computed values [*Davis*, 1979].

The goal of this paper is to review the results achieved thus far for evaluating the SAF and to discuss techniques for extending this effort. To this end, we first discuss the means that have been used of evaluating scattered fields from penetrable two-dimensional scatterers in a lossy medium. We shall then review briefly the pertinent solutions for the lossy media and finally indicate how they might be extended to the geometries of current interest.

The next sections of this paper focus attention on the analyses we have used to evaluate SAF's for lossy media. Later sections then introduce techniques that have been used for different problems that could be adapted to this purpose.

THE SCATTERING ATTENUATION FUNCTION

The scattering attenuation function is defined as

$$\mathrm{SAF} = E^s/E^i \quad \text{or} \quad H^s/H^i \quad \text{or} \quad U^s/U^i \tag{1}$$

where U^s is the scattered field from the two-dimensional target at the line source position, U^i is the radiated field of the line source at the image position as defined in Figure 1, and E and H represent electric and magnetic field intensities respectively.

The field parameter U can represent either the electric or the magnetic field intensity depending on whether the source is an electric or a magnetic line source. It is also possible to use line dipole sources. *Hohman* [1971] introduced a normalization that involved the magnetic fields in free space, i.e., Ampere's law. The normalization introduced here tends to cast the electrical parameters in a more usable form as we shall soon see.

The basic model shown in Figure 1 introduces a three-dimensional antenna at the image position. If the source antenna is also the receiving antenna, then

the normalized received voltage is approximately

$$V_R = (V_R'/V_T)\text{SAF} \tag{2}$$

The ray spreading in the plane of the paper of Figure 1 is contained in the factor V_R'. This also contains a spreading factor in the perpendicular plane which is canceled by the ray spreading contained in the factor E^I and is then replaced by the spreading factor inherent in E^S. If orthogonal transmit-receive dipole antennas are used rotated by 45°, then

$$V_R = \tfrac{1}{2}(V_R'/V_T)\text{SAF} \tag{3}$$

Strictly, (3) is valid only when the scattered field has a preferred polarization independent of the polarization of the incident field. This can be modified to account for the case where the scattered fields are simply different for different incident polarizations [*Burrell et al.*, 1979]. This model has been confirmed by comparison with a moment method solution using a 1000-m-long conducting cylinder as a target. The results for a video pulse radar agree within 0.6 dB where the received peak signals were 143 dB below the transmitted signal and the waveforms are identical. The reader is referred to *Burrell et al.* [1979].

The ratio V_R'/V_T can now be computed separately, and there is no need to restrict the actual antenna to either an infinitesimal dipole or a line source.

It is apparent that the SAF's are a function of depth d and the electrical parameters of the medium. However, these effects can be easily estimated with reasonable accuracy without repeating the entire analysis. Thus the SAF of a specific scatterer can be estimated reasonably accurately (within several decibels) as the range and electrical properties of the media vary.

The scattering attenuation function should not be seriously changed if a ground-air interface is included in the model, since it would influence the scattered field and the image field in the same manner. Two conditions must be met in order for the above assumption to be valid. First, there is no significant multiple target-interface interaction, and second, the lateral extent of the cylinder target is sufficiently small so that lateral waves on the surface are not significant. This could be relaxed to the extent that the extreme rays are not incident at the surface beyond the critical angle.

The guidelines to follow have been developed for the case where the pertinent scattering mechanisms involve internal reflections. The scattered fields will then be proportional to the Fresnel reflection coefficient.

Guideline 1. The level of the SAF in the target resonance region is changed, as the electrical parameters of the ambient medium are changed, by the change in the Fresnel reflection coefficient.

Guideline 2. The changes in the electrical properties of the ambient medium alter the loss contained in the SAF by an amount proportional to twice the distance from the leading portion of the (penetrable) target to the reference plane. This is because the reference field U^i is modified by this change.

Guideline 3. As the depth d is changed, the SAF is changed according to the approximate relation

$$U(R, d) = \left(\frac{R}{R + d}\right)^{1/2}$$

where R is the radius of curvature at the first stationary point on the target. This is based on geometrical optics and assumes either that this specular scatterer is dominant, which is usually the case for a lossy medium, or that $R \ll d$.

These guidelines have been used for circular tunnels [*Burrell et al.*, 1979] and have worked very well for the relations of the SAF as a function of media and depth. Thus the SAF parameter is somewhat more general than it would originally have appeared and in practice is a more useful concept than the conventional echo width.

Finally, one observes that the interface could have been incorporated in the model of Figure 1. There would be no substantial difficulty in analyzing the geometries of Figures 1*a* and 1*b*. However, if the antennas of Figure 1*c* are of finite extent, then very large computer running times are encountered [*Burrell and Peters*, 1979]. More recently, using techniques developed for stripline antennas, this difficulty has been largely eliminated [*Uzunoglu et al.*, 1979], but this has not been incorporated in these results.

MODAL SOLUTIONS

The sphere and the infinite cylinder represent classic shapes in the study of electromagnetic scattering. Prior to the advent of large digital computers it was most difficult to evaluate numerically the scattered fields of such lossy targets even when the ambient medium was free space. It is not surprising that, as *Parry and Ward* [1971] observe, *D'Yakonov* [1959*a*, *b*] 'has published a solution to scattering from a circular cylinder and a sphere in a conducting

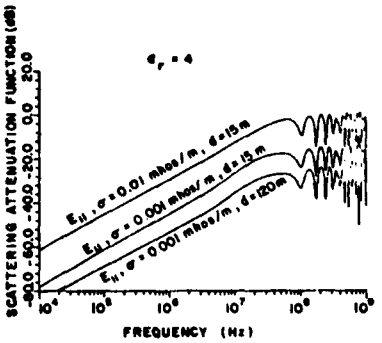

Fig. 2. Comparison of scattering attenuation function $E_{\parallel}$ for an electric line source for 1-m-radius tunnel for different depths d and conductivity σ shows that the primary effect of these parameters is to change the amplitude of the curve.

half-space, and we have yet to witness numerical results for either of these particular solutions.' *Ogunade* [1981] has attempted to extend D'Yakonov's solution to evaluate the fields at the surface of the earth using the circular cylinder as a target. However, in his assumed form of the scattered fields he has introduced a symmetry in the angle ϕ about ϕ_0 that is not actually present (see his equation (21) and his Figure 2). Even if this were corrected by introducing the terms $\sin n(\phi - \phi_0)$, the result would still not be correct except for the observation point directly above the buried cylinder. Also, as we have already observed, it is not always essential when considering the scattering problem to include the half space problem. Indeed, much valuable insight can be achieved in an economic manner if it is not included. Modal solutions for scattering from lossy circular cylinders in lossy half space excited by a line source are relatively straightforward to evaluate numerically using modern digital machines. However, the numerical computations become more complex when a finite antenna system (neither infinite nor infinitesimal) is introduced at the surface [*Burrell and Peters*, 1979]. There have been many analyses involving infinitesimal dipole sources located at the surface of a half space. Many of these include reflections from multiple layers in the lossy half space [*Wait*, 1958]. There have been few numerical solutions involving finite-sized antennas, particularly for the current distribution and the impedance, such as a resonant dipole at the surface of the lossy half space, primarily because of computation costs. This has been approximated by *Davis* [1979]. There is, however, a continued effort to generate new techniques which will ultimately eliminate this difficulty. *Howard* [1975], for example, uses fast Fourier transform (FFT) routines to obtain the scattered fields of a small radius conducting cylinder immersed in a lossy half space. There is at least one other modal solution that should be included in this discussion.

Wait's [1959] treatment of the scattered fields from an imperfectly conducing dike should also be included as a modal-based solution. His approach is a rather elegant preface to concepts now being introduced in the geometrical theory of diffraction (GTD) for the treatment of thin dielectric slabs and absorbers placed on conducting surfaces. We will later update this technique, show some newer, remarkably accurate results, and propose some possible extensions to this approach. The modal solution is applicable primarily to cylindrical shapes. With current computer technology there is no serious limitation on the size of the cylinder that can be treated. In this solution the incident wave is expanded in a set of cylindrical modes, and boundary conditions are applied to each mode individually to evaluate the coefficients of the scattered cylindrical modes. Summing the fields of each mode then gives the desired scattered fields.

Our recent computations have involved a number of solutions for the SAF of circular cylinders. Some examples are shown in Figures 2–4. Figure 2 gives the SAF for 1-m-radius tunnels of different depths and ambient media. It is left as an exercise to check the guidelines for depth and the media electrical parameter dependence given earlier. Figure 3 gives SAF's for lossy cylinders immersed in a lossy medium. These might represent tunnels filled with water or debris. Figures 4 and 5 give the SAF's for

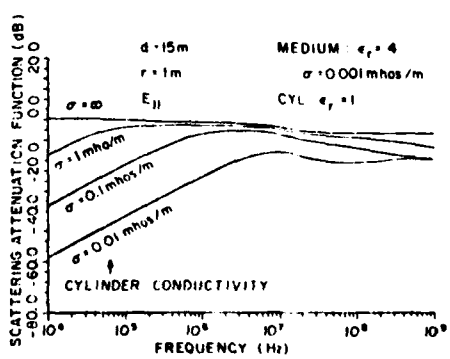

Fig. 3. Scattering attenuation function for lossy dielectric cylinders in a lossy medium for parallel electric polarization.

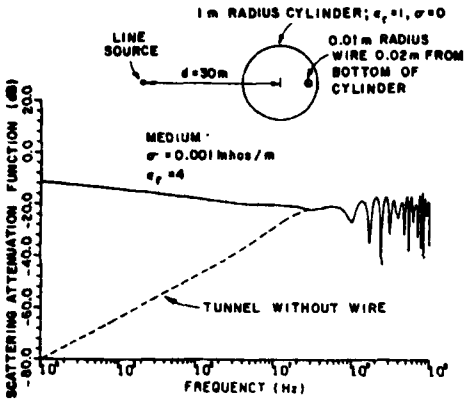

Fig. 4. Scattering attenuation function for air-filled cylinder with a perfectly conducting wire at the tunnel floor.

air-filled cylinders with a wire. The wires might represent a rail or a power line in the tunnel. Let E_1 denote the field of the line source near the dielectric cylinder without wire. Now let E_2 denote the field of a 1-A line source located within the dielectric cylinder at the position where we will later place the wire. The solution for E_2 makes use of the addition theorem [*Harrington*, 1961]. By superposition, the field of the exterior line source, radiating in the presence of the dielectric cylinder with interior wire, is given by $E = E_1 + IE_2$. The current I induced on the thin wire is determined by forcing E to vanish on the surface of the wire. The current is assumed to be distributed uniformly around the circumference of the wire. Finally, Figure 6 shows the SAF for a con-

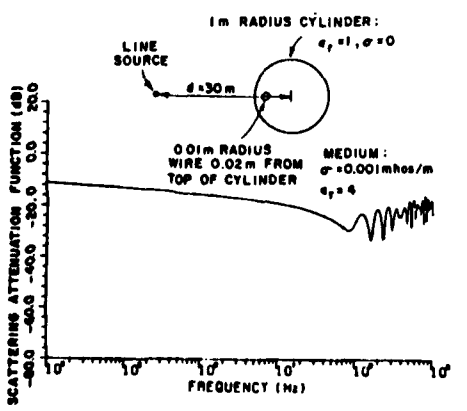

Fig. 5. Scattering attenuation function for air-filled cylinder with a perfectly conducting wire at the roof of the tunnel.

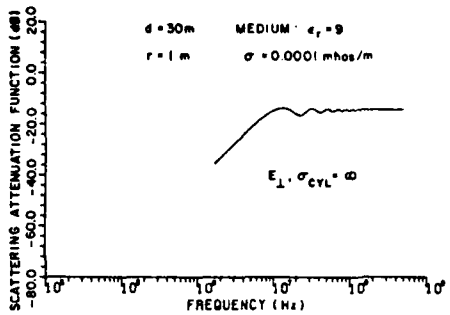

Fig. 6. Scattering attenuation function for perfectly conducting cylinder and perpendicular polarization in relatively loss free ground.

ducting cylinder immersed in a nearly lossless medium. The ripple in this case is caused by the creeping wave which is almost negligible even for this very lossless medium.

ALTERNATE TECHNIQUES AVAILABLE FOR SCATTERING FROM PENETRABLE CYLINDERS

There are perhaps three additional techniques available to evaluate scattered fields from penetrable cylinders. These include (1) moment method or integral equation solutions, (2) optical solutions, and (3) hybrid solutions. Each solution has its applications and its limitations, but they have not been developed at this time to their ultimate capacity for targets immersed in a lossy medium.

INTEGRAL EQUATION SOLUTIONS

There are two basic approaches using integral equations for the scattered fields of penetrable objects. One of these uses surface equivalence currents ($\mathbf{J} = \hat{n} \times \mathbf{H}$ and $\mathbf{M} = \mathbf{E} \times \hat{n}$) [*Harrington*, 1961] and requires the solution of coupled integral equations, one for the ambient medium and the other for the penetrable object [*Andreason*, 1965]. Matching the fields at the surface allows the unknown coefficients to be evaluated. This is quite similar to the Sommerfeld analysis of the half space. The other approach uses the so-called volume polarization currents to be discussed later [*Rhodes*, 1953; *Richmond*, 1965, 1966]. One of the major distinctions is that in the first case the boundary conditions are satisfied at the surface and in the second case they are satisfied throughout the volume. The choice of solution would

be associated largely with the electrical parameters, size, and shape of the penetrable body, and the decision would be based on the smallest matrix to be inverted.

For example, if a thin layer is to be treated, then the polarization current approach would be most appropriate. Alternately, if a large perturbation at an interface is to be analyzed, then the surface current would be more appropriate. Smaller objects or objects with a small dimension in terms of wavelength would require a smaller matrix if the volume polarization current approach is used. Since most moment method solutions are considered low-frequency techniques, then it seems appropriate to place emphasis on the polarization current density approach. An exception to this might be a gentle perturbation or 'swell' on an interface.

There is also an integral equation solution that has been designated as the T matrix used originally by *Waterman* [1965] for the analysis of electromagnetic scatterers. These solutions incorporated an extended boundary condition so that external to this boundary, outgoing cylindrical (or spherical) waves could be used. *Mei et al.* [1979] used a similar solution except that they introduced a finite difference solution to find the trial functions internal to the extended boundary. Again, these types of solutions would minimize the number of match points where the scatterer better fits the circular or spherical extended boundary.

Next we will outline the solution for a lossy dielectric of rather general cross section using the polarization current density approach.

MOMENT METHOD FOR ELECTRIC LINE SOURCE NEAR A LOSSY DIELECTRIC CYLINDER USING THE POLARIZATION CURRENT APPROACH

Consider an infinite electric line source with a uniform time harmonic current I_0. When radiating in a homogeneous medium with complex parameters μ and ε, this source generates the following incident field:

$$\mathbf{E}^i = -\hat{z} I_0 \eta\gamma K_0(\gamma\rho_s)/2\pi \tag{4}$$

where η and γ denote the intrinsic impedance and propagation constants of the ambient medium and K_0 denotes the modified Bessel function. The line source is located at (x_s, y_s) and is parallel with the z axis. The observer is located at (x, y), and

$$\rho_s = [(x-x_s)^2 + (y-y_s)^2]^{1/2} \tag{5}$$

Now consider the electric line source radiating in the presence of a nearby parallel dielectric cylinder. The field in this case is denoted by E, where

$$E = E^i + E^s \tag{6}$$

Since the field is z-polarized, scalar notation is suitable. The field E^s scattered by the dielectric cylinder may be generated by an equivalent polarization current density given by

$$J_{eq} = j\omega(\varepsilon_1 - \varepsilon)E \tag{7}$$

radiating in the homogeneous ambient medium $(\mu\varepsilon)$. The dielectric cylinder has parameters μ_1 and ε_1, and it may be inhomogeneous, but we assume $\mu_1 = \mu$. The current J_{eq} exists only in the dielectric region with permittivity ε_1. Since the field E is unknown, the current, J_{eq} is also unknown.

The scattered field is given by

$$E^s(x, y) = -\frac{\eta\gamma}{2\pi}\iint J_{eq}(x', y')K_0(\gamma\rho)\,dx'\,dy' \tag{8}$$

where the integration extends over the cross-sectional area of the cylinder and

$$\rho = [(x-x')^2 + (y-y')^2]^{1/2} \tag{9}$$

From (6) (8) we can derive the following integral equation:

$$\frac{J(x, y)}{j\omega(\varepsilon_1 - \varepsilon)} + \frac{\eta\gamma}{2\pi}\iint J(x', y')K_0(\gamma\rho)\,dx'\,dy' = E^i(x, y) \tag{10}$$

where $J = J_{eq}$. Now let us expand J in a series of basis functions as follows:

$$J(x, y) = \sum C_n F_n(x, y) \tag{11}$$

From (10) and (11),

$$\sum_n C_n\left[\frac{F_n(x, y)}{j\omega(\varepsilon_1 - \varepsilon)} + \frac{\eta\gamma}{2\pi}\iint F_n(x', y')K_0(\gamma\rho)\,dx'\,dy'\right] = E^i(x, y) \tag{12}$$

To determine the constants C_n, let us multiply (12) by a weighting function $G_m(x, y)$ and integrate over the cross-sectional area of the cylinder. In this manner we obtain the following system of simultaneous linear equations:

$$\sum_{n=1}^{N} C_n Z_{mn} = V_m \qquad m = 1, 2, \cdots N \tag{13}$$

$$Z_{mn} = \iint \frac{G_m(x, y)F_n(x, y)\,ds}{j\omega(\varepsilon_1 - \varepsilon)} + \frac{\eta\gamma}{2\pi}\iint\iint G_m(x, y) \cdot F_n(x', y')K_0(\gamma\rho)\,ds'\,ds \tag{14}$$

$$V_m = \iint G_m(x, y)E^i(x, y)\, ds \tag{15}$$

Numerical integration techniques are generally required to evaluate the integrals in (14) and (15). Matrix inversion yields the solution to (13), and then the scattered field is calculated via (8) and (11).

MOMENT METHOD FOR MAGNETIC LINE SOURCE NEAR A LOSSY DIELECTRIC CYLINDER

Consider an infinite magnetic line source with uniform time harmonic current distribution I_0. When radiating in a homogeneous medium with parameters μ and ε, this source generates the following incident field:

$$\mathbf{H}^i = \frac{-\gamma I_0 \hat{z}}{2\pi\eta} K_0(\gamma\rho_s) \tag{16}$$

$$E_x^i = \frac{\eta}{\gamma}\frac{\partial H_z}{\partial y} = \frac{\gamma I_0(y-y_s)K_1(\gamma\rho_s)}{2\pi\rho_s} \tag{17}$$

$$E_y^i = -\frac{\eta}{\gamma}\frac{\partial H_z}{\partial x} = -\frac{\gamma I_0(x-x_s)K_1(\gamma\rho_s)}{2\pi\rho_s} \tag{18}$$

The field scattered by the parallel dielectric cylinder (or radiated by the polarization current J in a homogeneous ambient medium) is given by

$$H_z^s(x, y) = \frac{\gamma}{2\pi}\iint [(y-y')J_x(x', y') - (x-x')J_y(x', y')]\frac{K_1(\gamma\rho)}{\rho}\, dx'\, dy' \tag{19}$$

where

$$\mathbf{J} = j\omega(\varepsilon_1 - \varepsilon)\mathbf{E}. \tag{20}$$

From (20) and Maxwell's equations,

$$J_x = j\omega(\varepsilon_1 - \varepsilon)E_x = \frac{(\varepsilon_1 - \varepsilon)}{\varepsilon_1}\frac{\partial H_z}{\partial y} \tag{21}$$

$$J_y = j\omega(\varepsilon_1 - \varepsilon)E_y = -\frac{(\varepsilon_1 - \varepsilon)}{\varepsilon_1}\frac{\partial H_z}{\partial x} \tag{22}$$

From (19)–(22),

$$H_z^s(x, y) = \frac{\gamma}{2\pi}\iint \frac{(\varepsilon_1 - \varepsilon)}{\varepsilon_1}\left[(y-y')\frac{\partial H_z}{\partial y'} + (x-x')\frac{\partial H_z}{\partial x'}\right]\frac{K_1(\gamma\rho)}{\rho}\, dx'\, dy' \tag{23}$$

The incident, scattered, and total fields are related as follows:

$$H = H^i + H^s \tag{24}$$

From (23) and (24) we obtain the following integral equation:

$$H(x, y) = H^i(x, y) + \frac{\gamma}{2\pi}\iint \frac{(\varepsilon_1 - \varepsilon)}{\varepsilon_1}\left[(y-y')\frac{\partial H}{\partial y'} + (x-x')\frac{\partial H}{\partial x'}\right]\frac{K_1(\gamma\rho)}{\rho}\, dx'\, dy' \tag{25}$$

Now let us expand the unknown function H in a series as follows:

$$H(x, y) = H_z(x, y) = \sum C_n F_n(x, y) \tag{26}$$

where the functions F_n are called the basis functions. From (25) and (26),

$$\sum C_n F_n(x, y) = H^i(x, y) + \frac{\gamma}{2\pi}\sum C_n \iint \frac{(\varepsilon_1 - \varepsilon)}{\varepsilon_1} \cdot \left[(y-y')\frac{\partial F_n}{\partial y'} + (x-x')\frac{\partial F_n}{\partial x'}\right]\frac{K_1(\gamma\rho)}{\rho}\, dx'\, dy' \tag{27}$$

To determine the constants C_n, we multiply (27) by a weighting function $G_m(x, y)$ and integrate over the cross-sectional area of the dielectric cylinder. This yields the following system of simultaneous linear equations:

$$\sum_{n=1}^{N} C_n Z_{mn} = V_m \qquad m = 1, 2, \cdots N \tag{28}$$

$$Z_{mn} = \iint G_m(x, y)F_n(x, y)\, ds - \frac{\gamma}{2\pi}\iint\iint \frac{(\varepsilon_1 - \varepsilon)}{\varepsilon_1} G_m(x, y) \cdot \left[(y-y')\frac{\partial F_n}{\partial y'} + (x-x')\frac{\partial F_n}{\partial x'}\right]\cdot\frac{K_1(\gamma\rho)}{\rho}\, ds'\, ds \tag{29}$$

$$V_m = \iint G_m(x, y)H^i(x, y)\, ds \tag{30}$$

Equation (28) is solved by matrix inversion or equivalent techniques, and then the scattered field is calculated via (23) and (26).

Figure 7 shows the scattering attenuation function as defined in (1) for a square cylinder as obtained with the general approach just outlined. Hohman also made some scattered field computations from a square conducting medium, but these did not extend into the resonance region.

Use of the SAF of Figure 1 in the model of Figure 1 has yielded reasonable agreement with measured results as obtained using a video pulse radar [*Davis*, 1979].

INSULATED FINITE LENGTH WIRES IN A CONDUCTING MEDIUM

Conducting finite length wires immersed in a conducting medium can be readily analyzed using con-

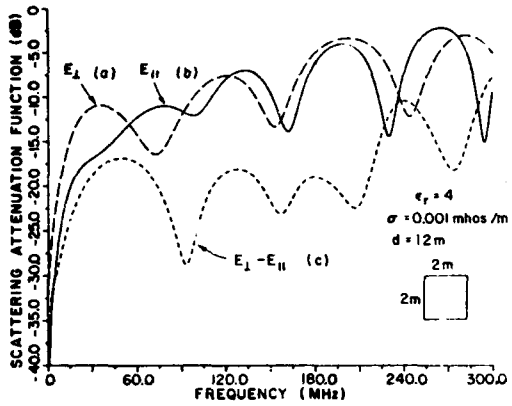

Fig. 7. Composite scattering function of 2-m-square air-filled tunnel obtained by a polarization current moment method solution. $E_\perp - E_\parallel$ represents the SAF for a crossed dipole antenna (see equation (3)).

ventional moment method techniques. One such result has already been noted. We have also considered infinite wires immersed in a circular tunnel using modal techniques. The solution to be discussed here is that of an insulated finite length wire. A coaxial-like mode is assumed where the volume polarization currents are placed in the dielectric shell and surface currents are on the surface of the wire. The electric field in the dielectric shell is assumed to be radial yielding polarization currents

$$J_\rho = -(\epsilon_2 - \epsilon)I'(l)\frac{1}{2\pi\epsilon_2\rho} \tag{31}$$

where $I(l)$ is the current on the wire. Designating this current in the dielectric shell as a tubular expansion dipole, one needs to include the mutual impedance between the nth tubular expansion dipole and the mth filamentary dipole (in the lossy medium) in the mutual impedance Z_{mn}. The moment method solution then proceeds in a normal fashion. The reader is referred to *Richmond and Newman* [1976] for further details. This approach has been tested by evaluating the impedance of insulated wire antennas. A typical example is shown in Figures 8 and 9. This same approach has been used to find the scattered fields from an insulated conducting wire in a homogeneous medium. In this case, we present the scattering attenuation function results, as incorporated in the received voltage at the terminals of the receiving antenna shown in Figure 1. The source in this case is a Gaussian pulse which contains a rather wide spectrum. The steps in the analysis include taking the FFT of the transmitting pulse, evaluating the component terms illustrated in Figure 1, and taking the inverse FFT to obtain the received voltage waveforms now shown in Figure 10. The spectrum of several of these waveforms is shown in Figure 11, where 'tunnel length' represents the length of the insulated buried wire.

HYBRID SOLUTIONS

Hybrid solutions have been used to analyze various geometries that may not be treated by the usual moment method solutions. They have been used to treat the infinite conducting wedge [*Burnside et al.*, 1975] and an initial solution for an infinite dielectric wedge. They have not yet been used for the treatment of objects immersed in a lossy medium.

The hybrid solution is a combination of a moment method solution with another solution where the unknown fields outside a restricted region can be represented by a field of known functional form multiplied by an unknown constant. One of the original solutions took the form illustrated in Figure 12. The currents on the surface of the conducting wedge outside the encircled region can be written in the form

$$\mathbf{J}^{\mathrm{GTD}} = \mathbf{J}^i + \mathbf{J}^r + (\hat{n} \times \hat{z})\frac{Ce^{-jk\rho}}{\rho^{1/2}} \tag{32}$$

where $\mathbf{J}^i = \hat{n} \times \mathbf{H}^i$ and $\mathbf{J}^r = \hat{n} \times \mathbf{H}^r$. $\mathbf{H}^i$ and $\mathbf{H}^r$ are the incident and reflected magnetic field intensities respectively; the only unknown is the constant C.

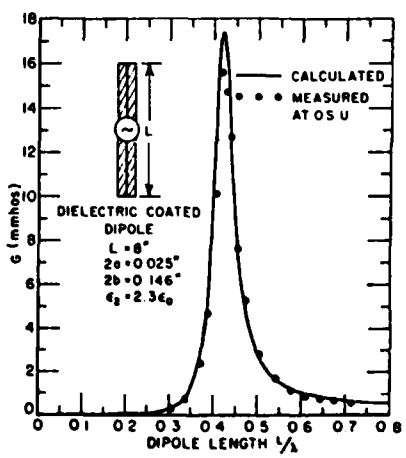

Fig. 8. The conductance of an insulated dipole plotted versus its length in wavelengths.

The surface currents inside the encircled region are unknown and are evaluated along with the constant C using conventional moment method techniques. *Harrington* [1968] gives as an integral equation for the total current density J:

$$\mathbf{J} = -\left[H_z^i + \hat{z} \cdot \nabla \times \frac{1}{4j} \int_L \mathbf{J} H_0^{(2)}(k|\rho - \rho'|)\, dl'\right] \tag{33}$$

where L is taken about the perimeter of the conducting surface. Inside the encircled region the currents can be represented using subsectional bases. Outside the encircled region they are represented by the GTD currents given by (32). For the lossless media, this will involve integrations along the surface of the form

$$\int_{\rho_c}^{\infty} \frac{jk}{4} \frac{e^{-jk\rho'}}{\rho'^{1/2}} H_1^{(2)}(k|\rho - \rho'|)\, d\rho' \tag{34}$$

where ρ' is taken along the surface of the wedge.

As *Burnside et al.* [1975] observe, this integration need not be carried to ∞ because of the decaying nature of the Hankel function.

Next, one can consider the case of the conducting wedge in a lossy medium as a first step in considering lossy wedges immersed in a lossy medium as the external medium becomes lossy ($jk \rightarrow -\alpha - jk$); this integral becomes negligible for much smaller values of ρ, and thus the solution is simplified. If the loss is more than marginal, then indeed one could find the fields diffracted by the edge of the wedge without using the hybrid approach, unless one is particularly interested in the fields along the surface of the wedge. *Aas* [1975] has used additional terms in J^{GTD} of the form $C_2 e^{-jkr}$ and $C_3 e^{-jk\rho}/\rho^{\frac{1}{2}}$ to include the cases of

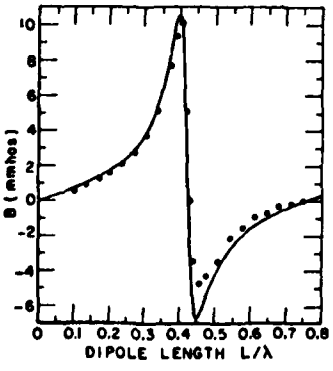

Fig. 9. The susceptance of the insulated dipole, shown in Figure 8, plotted versus its length in wavelengths.

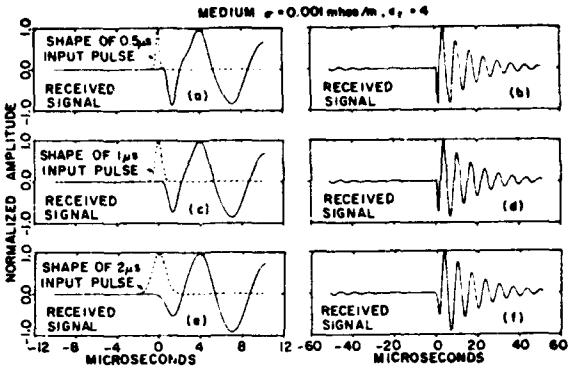

Fig. 10. Signals received on a 50-m orthogonal dipole antenna system 50 m from 300 m long, 0.1-m-radius tunnel containing a 0.01-m-radius wire on its axis. (*a* and *b*) The early time behavior and the complete received signal respectively for a 0.5-μs Gaussian input pulse. (*c–d* and *e–f*) The signals for 1-μs and 2-μs input pulses respectively.

grazing incidence and also polarization parallel to the surface.

Wu and Tsai [1977] have adapted this approach for the case of a dielectric wedge. They have used

$$\mathbf{J}^{GTD} = \mathbf{J}^i + \mathbf{J}^r \tag{35}$$

They have included only first-order geometrical optics fields for the region far away from the tip of the wedge, primarily because there is not yet a solution for the diffracted fields of a dielectric wedge.

At first glance, it would appear that the coupled integral equation approach would be more suitable for the hybrid approach since it would be more suitable for defining a wave on the surface of the wedge comparable to the hybrid analysis of the conducting wedge. They observe that the solution could be improved by including multiple reflections internal to the wedge. They also note that it would be improved when the tip diffraction term, once its form is known, is included.

OPTICAL SOLUTIONS

The optical solutions generally analyze scattering using ray techniques such as conservation of energy in a ray tube, plane wave refraction and reflection coefficients, caustics, etc.

MODIFIED GEOMETRICAL OPTICS METHOD

For example, some of the earliest solutions of this type focused attention on the scattered fields of di-

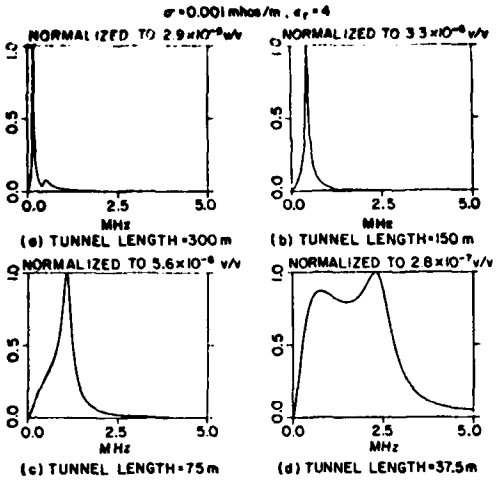

Fig. 11. Magnitude of transmission transfer function for 50-m-long, 0.002-m-radius uninsulated dipole antenna system 50 m from a finite length tunnel for various tunnel lengths. The tunnel has a radius of 0.1 m and contains a 0.01-m-radius wire at its center.

electric spheres and cylinders [*Kouyoumjian et al.*, 1963; *Peters et al.*, 1965]. Analyses of this type were designated as the modified geometrical optics method. Some of the ray mechanisms that were considered are illustrated in Figure 13. Ray 1 in Figure 13 is an externally reflected ray, ray 2 is the axial internally reflected ray, and ray 3 represents two nonaxial rays. One of these is shown in Figure 14 and is known as the glory ray. It has an apparent focus or caustic located a distance ρ_1 from the surface as shown. Figure 15 shows the geometry of the stationary or rainbow ray. The analysis included the

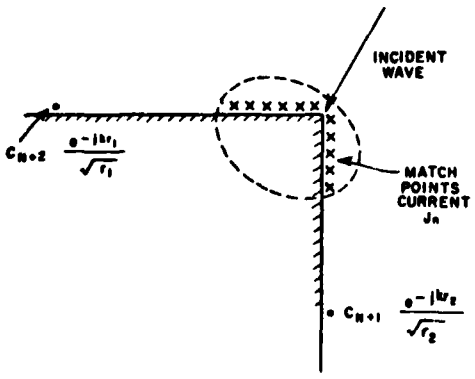

Fig. 12. Geometry for hybrid solution for the conducting wedge.

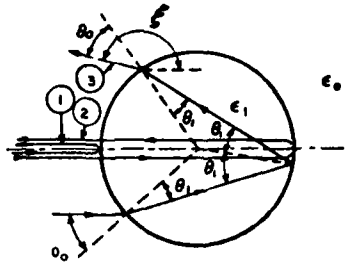

Fig. 13. On the general ray path.

electrical path lengths, the caustics, and multiple internally reflected rays. Figure 16 shows the comparison of the approximate echo width of several cylinders whose relative permittivities are 0.50 and 0.75 with those obtained from the exact solution. These examples were chosen since they might be more representative of a sewer pipe or a plastic gas pipe, tunnel, etc., than other values that have also been obtained. The analysis becomes more complex as $\varepsilon_r = \varepsilon_1/\varepsilon_0$ shown in Figure 13 becomes large with respect to 1. *Ianda and Plonus* [1969] have criticized this approach and claimed that surface waves are needed to complete the picture. There is one other mechanism that is possible, a lateral (or up, over, and down) wave. This would be applicable when the index of refraction for the cylinder is greater than that of the ambient medium. At any rate for $\varepsilon_r = 2.56$, *Barrick* [1968] included the following rays: (1) externally reflected ray, (2) single-bounce axial ray, (3) triple-bounce axial ray, (4) single-bounce glory ray, and (5) single-bounce stationary ray. He obtained reasonably good agreement between the modified geometrical optics solution and the exact solution except for raggedness in the frequency dependent curves of the exact solution. He reported that

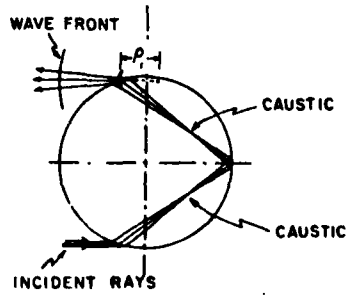

Fig. 14. Wave front of single-bounce glory ray.

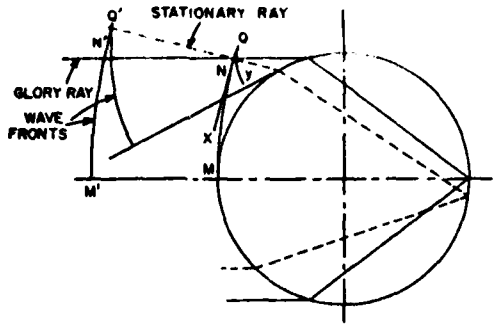

Fig. 15*a*. Equiphase surfaces associated with single-bounce *stationary ray*.

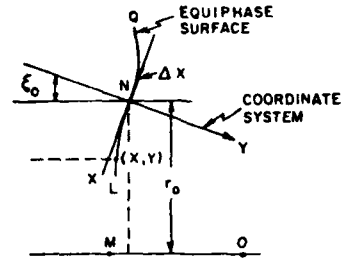

Fig. 15*b*. Enlarged figure about point N for the equiphase surface of single-bounce stationary ray.

the addition of small losses eliminated this ragged characteristic. Including other rays of the type listed did not introduce such a behavior, and he attributed it to a much higher order periodic type of trapped mode. This is probably the lateral wave mechanism.

This type of solution has been applied to a variety of dielectric materials where the targets are generally circular cylinders and spheres. There is, however, nothing that restricts it to these geometries. It could be applied for almost any shape exclusive of caustic regions where special techniques are needed to evaluate the fields. While all analyses thus far have considered only lossless targets in a lossless medium losses can be accounted for in terms of an attenuation along the pertinent ray paths, etc. These ray paths may lie in the ambient medium and on or inside the scatterer. The introduction of loss may also generate additional ray paths. Of course, reflection coefficients, etc., will be modified. It should be noted that such solutions would generally be simpler since multiple internal reflections in a lossy cylinder would be attenuated and would reduce the number of internal rays that need be included in the solution.

GEOMETRICAL THEORY OF DIFFRACTION SOLUTION

A more recent optical solution makes use of some of the concepts of edge diffraction [*Burnside and Pathak*, 1981]. Consider the diffracted fields from the edge of a conducting half plane given by

$$\begin{pmatrix} H^d \\ \text{or} \\ E^d \end{pmatrix} = \begin{pmatrix} H^i \\ \text{or} \\ E^i \end{pmatrix} [D(s, s', \phi - \phi') \pm D(s, s', \phi + \phi')] \quad (36)$$

where E^i and H^i are the fields of the incident wave, D is the diffraction coefficient, and the geometry is given in Figure 17. The incident fields are shielded at $\phi - \phi' = \pi$, which is called the shadow boundary. The image (or reflected fields from the half plane) fields do not exist for $\phi + \phi' = \pi$. Thus a reflection boundary exists at $\phi + \phi' = \pi$. The diffraction coefficients $D(s, s', \phi - \phi')$ and $D(s, s, \phi + \phi')$ are intimately associated with the incident and reflection shadow boundaries respectively. The diffracted fields given by $D(s, s', \phi + \phi')$ are proportional to the discontinuity of the fields at the shadow boundary (SB), and the diffracted fields given by $D(s, s', \phi + \phi')$ are proportional to the discontinuity at the reflection boundary (RB).

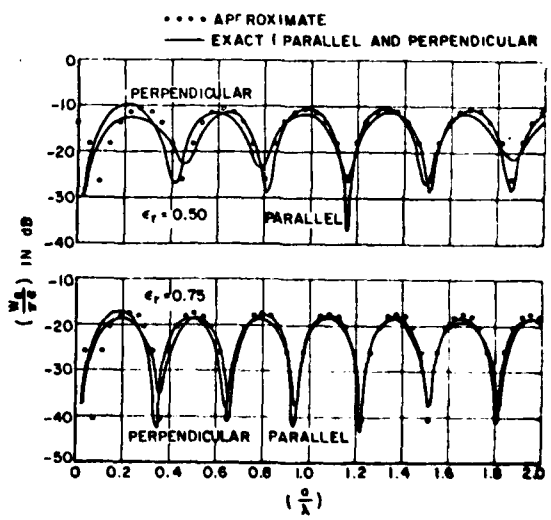

Fig. 16. Comparison of exact and approximate backscatter echo width of an infinite circular dielectric cylinder for relative permittivity $\epsilon_r = 0.50, 0.75$.

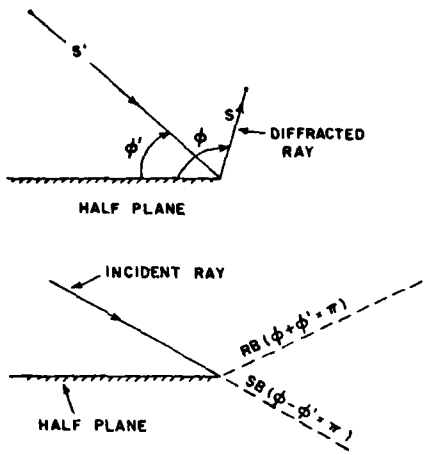

Fig. 17. Edge-diffracted ray geometry. RB is reflection boundary; SB is shadow boundary.

Suppose now we permit the half plane to be thin and penetrable. Then there is a partial reflection and a partial transmission at the half plane as represented by Figure 18. Now (36) takes the form

$$\begin{Bmatrix} H^d \\ \text{or} \\ E^d \end{Bmatrix} = \begin{Bmatrix} H^i \\ \text{or} \\ E^i \end{Bmatrix} [(1 - T)D_{\substack{s\\h}}(s, s', \phi - \phi') + R_{\substack{s\\h}}D(s, s', \phi + \phi')] \tag{37}$$

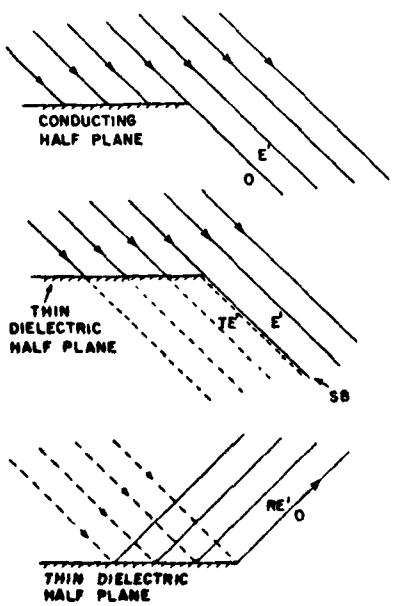

Fig. 18. Optical boundaries for dielectric half plane.

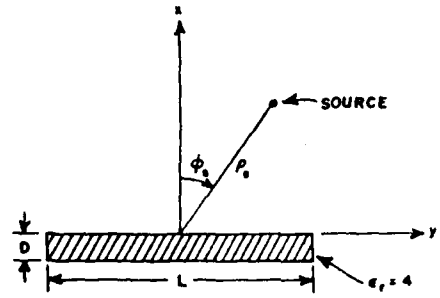

Fig. 19. Geometry used for GTD-moment method (MM) comparison.

where $(1 - T) = R$ represents the discontinuity of fields at the shadow and reflection boundaries respectively. This type of solution has been applied to the case of a thin dielectric slab. *Burnside and Pathak* [1981] have calculated the far field radiated fields for a number of two-dimensional geometries. An example of this geometry is given in Figure 19. A typical result is shown in Figure 20 where this GTD solution is compared with the moment method solution.

We observe that the results obtained herein do confirm the accuracy of the method. The fact that there is agreement over the entire pattern also removes the potential restriction discussed by *Wait* [1959] concerning the location of the source and observation point. This is accomplished by the appropriate modification of the diffracted fields associated with both the shadow and the reflection boundaries.

A significant factor here is that the scattered fields can indeed be represented by a discrete shadow boundary and by the same form of diffracted fields as for the conducting shape. If the same basic postulate is made for penetrable wedge geometries with differ-

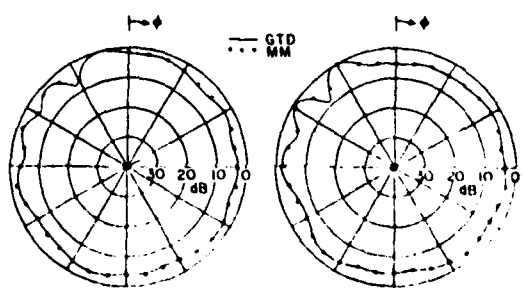

Fig. 20. GTD-MM comparison with electric line source using geometry shown in Figure 19 with $L = 2.0\lambda$, $D = 0.05\lambda$, $\rho_s = 2.0\lambda$ (Left) $\phi_s = 20°$ and (right) $\phi_s = 40°$.

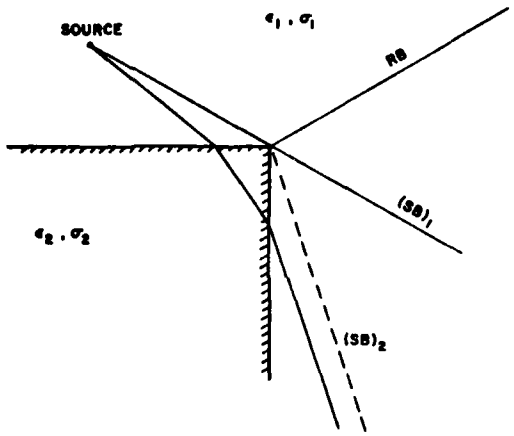

Fig. 21. Some reflection and shadow boundaries for a penetrable wedge.

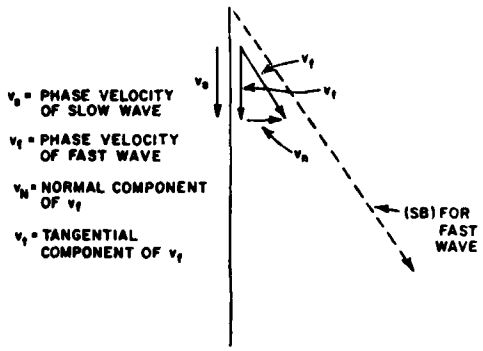

Fig. 23. Phase velocities of a wave along the surface of the wedge of Figure 22.

ent angles, it may become possible to construct solutions for more general shapes. In the following paragraphs, we outline some of the considerations that might be used to obtain GTD type solutions to more complex geometries. The reader is cautioned that these are merely presented here as untested postulates.

The principle limitation on the results shown in Figure 20 is the thickness of the slab. For thicker slabs or for subsurface geometries that might be of interest, the index of refraction and the angle of incidence will introduce additional limitations. Consider, for example, the geometry of Figure 21. For this case, it might appear that the boundary conditions are essentially those that have already been stated and used in (37), and indeed for diffracted fields in the vicinity of the reflection boundary (where the second term of (37) is dominant) this may represent a valid approximation. However, for fields in the vicinity of the shadow boundary (where the first term in (37) is dominant) this approach is clearly erroneous. Also, since the phase velocities of the 'ray optical fields' in the two media must differ, it is impossible to satisfy the boundary conditions along the surface by such fields. Thus we now must introduce the additional complication of some type of 'trapped' or lateral wave field. Thus the possibility of a Zenneck type wave [*Hill and Wait*, 1978, 1980] must be considered. These fields would be represented by 'complex rays.' This subject has been studied in considerable depth by Felson and his co-workers [*Felson*, 1981].

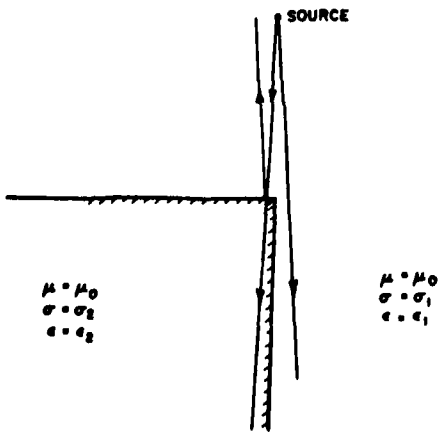

Fig. 22. Grazing incidence on the face of a penetrable wedge.

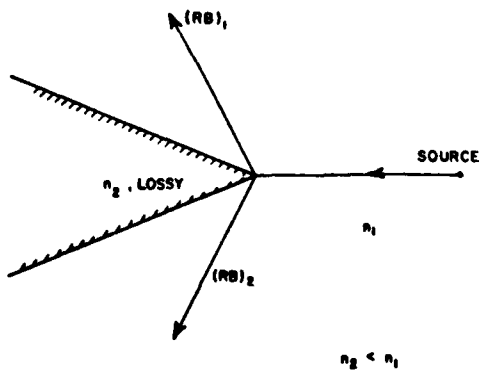

Fig. 24. A penetrable wedge geometry where the GTD solution should give good results.

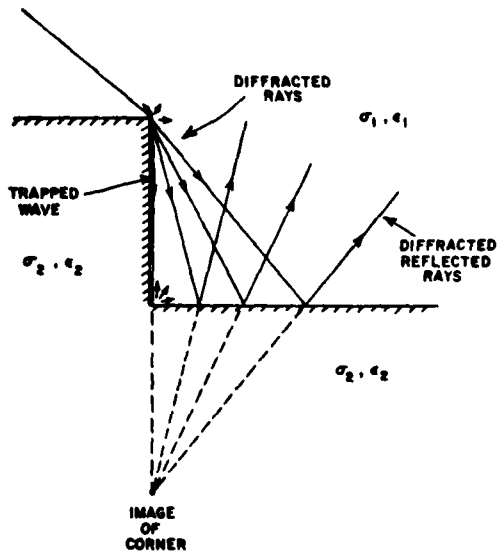

Fig. 25. Suggested ray configuration for a simplistic fault geometry where current GTD solution is appropriate.

Looking further at the geometry of the vertical interface of Figure 21 as illustrated in Figure 22, we observe that the phase velocity of the wave at the surface on the low index of refraction side has the appearance of a fast wave. Its phase velocity must have a component, not only along the vertical interface but also perpendicular to it. It would consequently appear as a shadow boundary as shown in Figure 23.

The launching properties of such a field should be studied carefully using the hybrid solutions already discussed. Once these are adequately understood, they would be used as a tool for studying more complex geometries.

Note also that the various boundaries are associated with different wedge surfaces. For example, $(SB)_2$ is clearly associated with the vertical suface of Figure 21. Thus once the equivalence currents are evaluated for the wedge, one could assume that the equivalence currents on the vertical surface would contribute to the fields $(SB)_2$ and its associated diffracted fields. One could further refine this model by neglecting the optical fields on the vertical edge and repeating the hybrid solution. In this manner, one could hope to construct a solution for a dielectric wedge in a GTD format.

In Figure 21 we recall that there now are two shadow boundaries at different angles. From a geometric optics viewpoint, there is a void between these two boundaries. This is clearly a more complex case. It becomes even more complex if the line source is not in the far field since the fields of rays associated with $(SB)_2$ are not homogeneous because they are dependent on various incidence angles at the surface. One could make various postulates as to the form of these diffracted fields. However, at this time, not enough has been achieved to be realistic. Perhaps the proper approach, barring the development of an adequate modal solution, would be to extend the hybrid solution and seek GTD-like representations with the appropriate uniform behavior to represent them as rays.

Figure 24 illustrates an example where reasonable results might be obtained for the space designated as η_1 using the approach given by Burnside. The overly stringent requirement that $\eta_1 < \eta_2$ implies that there are no multiply reflected rays. The diffracted fields from any internal shadow boundaries would tend to remain inside the wedge. The external diffracted fields would be those of the conducting wedge multiplied by the appropriate reflection coefficients. These solutions, once developed, should prove useful for providing building blocks to more complex geometries. For example, Figure 25 sketches some of the additional mechanisms that might appear in a 'fault-like' geometry. The rays diffracted by the upper corner appear after reflection from the lower interface to be emanating from the image shown. Of course, improved values are needed for the fields diffracted by the upper corner. Evaluating the reflection of the trapped wave also would require 'additional study.' These would probably give fields of lower value because of loss.

CONCLUSIONS

The scattering attenuation function has been defined for the scattering from two-dimensional targets using finite size antennas. Some results have been presented for the SAF of targets in a lossy medium. Possible extensions of existing methods for this purpose have also been discussed.

Acknowledgments. The authors are indebted to W. D. Burnside for helpful suggestions and permission to use some of his recent results. This work was supported in part by the Department of Electrical Engineering, ElectroScience Laboratory, Ohio State University, Columbus, Ohio, and in part by the Army Research Office, contract DAAG29-79-C-0082.

REFERENCES

Aas, J. A. (1975), Control of electromagnetic scattering from wing profiles by impedance loading, *Rep. 3424-4*, ElectroSci. Lab., Ohio State Univ., Columbus.

Andreason, M. G. (1965), Scattering from cylinders with arbitrary surface impedance, *Proc. IEEE 53*(8), 812–817.

Barrick, D. E. (1968), A note on scattering from dielectric bodies by the modified geometrical optics method, *IEEE Trans. Antennas Propag.*, *16*(2), 275–277.

Burnside, W. D., and P. H. Pathak (1981), High frequency scattering by a thin dielectric slab, paper presented at Second International Conference on Antennas and Propagation, Part I, Antennas, University of York, United Kingdom.

Burnside, W. D., C. L. Yu, and R. Marhefka (1975), A technique to combine the geometrical theory of diffraction and the moment method, *IEEE Trans. Antennas Propag.*, *23*(4), 551–558.

Burrell, G. A., and L. Peters, Jr. (1979), Pulse propagation in lossy media using the low frequency window for video pulse radar application, *Proc. IEEE*, *67*(7), 981–990.

Burrell, G. A., J. H. Richmond, L. Peters, Jr., and H. B. Tran (1979), A scattering model for detection of tunnels using video pulse radar systems, in *Acoustic, Electromagnetic, and Elastic Wave Scattering—Focus on the T-Matrix Approach*, Pergamon, New York.

Davis, C. W., III (1979), A computational model for subsurface propagation and scattering for antennas in the presence of a conducting half space, Ph.D. dissertation, Ohio State Univ., Columbus.

D'Yakonov, B. P. (1959*a*), The diffraction of electromagnetic waves by a circular cylinder in a homogeneous half space, *Bull. Acad. Sci. USSR, Geophys. Ser.*, *9*, 950–955.

D'Yakonov, B. P. (1959*b*), The diffraction of electromagnetic waves by a sphere located in a half space, *Bull. Acad. Sci. USSR, Geophys. Ser.*, *11*, 1120–1125.

Felson, L. B. (1981), Ray and modal approaches to guided wave propagation, paper presented at the 20th URSI General Assembly, Washington, D. C.

Harrington, R. F. (1961), *Time Harmonic Electromagnetic Fields*, McGraw-Hill, New York.

Harrington, R. F. (1968), *Field Computation by Moment Methods*, Macmillan, New York.

Hill, D. A., and J. R. Wait (1978), Excitation of the Zenneck surface wave by a vertical aperture, *Radio Sci.*, *13*(6), 969–977.

Hill, D. A., and J. R. Wait (1980), On the excitation of the Zenneck surface wave over the ground at 10 MHz, *Ann. Telecommun.*, *35*, 179–182.

Hohman, G. W. (1971), Electromagnetic scattering by conductors in the earth near a line source of current, *Geophysics*, *36*, 101–131.

Hohman, G. W. (1975), 3-D, IP, EM modeling, *Geophysics*, *40*(2), 309–324.

Howard, A. Q. (1975), A canonical solution to the three dimensional electromagnetic prospecting problem, *Radio Sci.*, *10*(4), 461–471.

Ianda, H., and M. A. Plonus (1969), Numerical results for backscattering from large high density dielectric spheres, *Proc. IEEE*, *67*(6), 1192–1193.

Kouyoumjian, R. G., D. T. Thomas, and L. Peters, Jr. (1963), A modified geometrical optics method for scattering by dielectric bodies, *IEEE Trans. Antennas Propag.*, *11*(11), 690–703.

Mei, K. K., J. F. Hunka, and S. K. Chang (1979), Recent developments in the unimoment method, in *Acoustic Electromagnetic and Elastic Wave Scattering—Focus on the T-Matrix Approach*, edited by V. K. and V. J. Varadan, pp. 485–506, Pergamon, New York.

Ogunade, S. O. (1981), Electromagnetic response of an embedded cylinder for line current excitation, *Geophysics*, *46*(1), 45–52.

Parry, J. R., and S. H. Ward (1971), Electromagnetic scattering from cylinders of arbitrary cross section in a conductive half space, *Geophysics*, *36*(1), 67–100.

Peters, L., Jr., T. Kawano, and W. G. Swarner (1965), Approximations for dielectric and plasma scatterers, *Proc. IEEE*, *53*(8), 882–892.

Pridmore, D. F. (1978), Three dimensional modeling of electrical and electromagnetic data using the finite element method, Ph.D. thesis, Univ. of Utah, Salt Lake City.

Rhodes, D. R. (1953), On the theory of scattering by dielectric bodies, *Rep. 475-1*, Antenna Lab., Ohio State Univ., Columbus.

Richmond, J. H. (1965), Scattering by a dielectric cylinder of arbitrary cross section, *IEEE Trans. Antennas Propag.*, *13*(3), 334–341.

Richmond, J. H. (1966), T. E. scattering by a dielectric cylinder of arbitrary shape, *IEEE Trans. Antennas Propag.*, *14*(4), 460–464.

Richmond, J. H. (1978), Computer solutions for use in estimating the progress of in-site coal gasification, *Rep. 784491-5*, ElectroScience Lab., Ohio State Univ., Columbus.

Richmond, J. H., and E. H. Newman (1976), Dielectric coated antennas, *Radio Sci.*, *11*(1), 13–20.

Stoyer, C. H., and R. J. Greenfield (1976), Numerical oscillations of the response of a two dimensional earth to an oscillating magnetic dipole source, *Geophysics*, *41*, 519–520.

Uzunoglu, N. K., N. G. Alexopoulos, and J. G. Fikioris (1979), Radiation properties of microstrip dipoles, *IEEE Trans. Antennas Propag.*, *27*(6), 853–857.

Wait, J. R. (1958), Induction by an oscillating magnetic dipole over a two layer ground, *Appl. Sci. Res., Sect. B*, *7*, 73–80.

Wait, J. R. (1959), On the electromagnetic response of an imperfectly conducting thin dyke, *Geophysics*, *24*(1), 167–171.

Ward, S. H. (1980), Electrical, electromagnetic and magnetotelluric methods, *Geophysics*, *45*(11), 1659–1666.

Waterman, P. C. (1965), Matrix formulation of electromagnetic scattering, *Proc. IEEE*, *53*(8), 805–812.

Wu, T. K., and L. L. Tsai (1977), Scattering by a dielectric wedge: A numerical solution, *IEEE Trans. Antennas Propag.*, *25*(4), 570–571.

APPENDIX F

PROPAGATION OF SURFACE WAVES ON A BURIED COAXIAL CABLE

WITH PERIODIC SLOTS

(ABSTRACT)

PROPAGATION OF SURFACE WAVES ON A BURIED COAXIAL CABLE WITH PERIODIC SLOTS*

J.H. Richmond

The Ohio State University ElectroScience Laboratory
Department of Electrical Engineering
Columbus, Ohio 43212

ABSTRACT

Consider a horizontal coaxial cable with periodic slots in the outer conductor. This "leaky cable" is buried in the earth as one component of an intruder detection system. We develop the theory for surface-wave propagation on the cable in the presence of the planar air-earth interface. Numerical results are included for the phase velocity and attenuation constant as functions of the various parameters. Data are presented for the electric field strength at the air-earth interface, and the electric field distribution in the air region above the buried cable.

---

*This work was supported in part by Waterways Experiment Station, Environmental Systems Division under Contract DACA39-80-K-0001 and The Department of the Army, U.S. Army Research Office under Contract DAAG29-79-C-0082 with The Ohio State University Research Foundation.